Journal of Chromatography A

Characterisation of selenium and tellurium nanoparticles produced by Aureobasidium pullulans using a multi-method approach.

--Manuscript Draft--

Manuscript Number:	JCA-20-1167R2
Article Type:	Full length article
Keywords:	Biogenic nanoparticles; selenium; tellurium; AF4-UV-MALS; ICP-MS/MS; spICP-MS
Corresponding Author:	Kenneth C Nwoko, PhD University of Aberdeen Aberdeen, UNITED KINGDOM
First Author:	Kenneth C Nwoko, PhD
Order of Authors:	Kenneth C Nwoko, PhD
	Xinjin Liang, PhD
	Magali Perez, PhD
	Eva M Krupp, PhD
	Geoffrey M Gadd, PhD
	Joerg Feldmann, PhD
Abstract:	Aureobasidium pullulans was grown in liquid culture media amended with selenite and tellurite and selenium (Se) and tellurium (Te) nanoparticles (NPs) were recovered after 30 d incubation. A separation method was applied to recover and characterise Se and Te NPs by asymmetric flow field flow fractionation (AF4) with online coupling to multi-angle light scattering (MALS), ultraviolet visible spectroscopy (UV-Vis), and inductively coupled plasma mass spectrometry (ICP-MS) detectors. Additional characterisation data was obtained from transmission electron microscopy (TEM), and dynamic light scattering (DLS). Solutions of 0.2% Novachem surfactant and 10 mM phosphate buffer were compared as mobile phases to investigate optimal AF4 separation and particle recovery using Se-NP as a model sample. 88 % recovery was reported for 0.2 % Novachem solution, compared with 50 % recovery for phosphate buffer. Different Crossflow (C flow) rates were compared to further investigate optimum separation, with recoveries of 88% and 30% for Se-NPs, and 90% and 29% for Te-NPs for 3.5 mL min -1 and 2.5 mL min -1 respectively. Zeta-potential (ZP) data suggested higher stability for NP elution in Novachem solution, with increased stability attributed to minimised NP-membrane interaction due to PEGylation. Detection with MALS showed monodisperse Se-NPs (45-90 nm) and polydisperse Te-NPs (5-65 nm).Single particle ICP-MS showed mean particle diameters of 49.7±2.7 nm, and 135 ± 4.3 nm, and limit of size detection (LOSD) of 20 nm and 45 nm for Se-NPs and Te-NPs respectively. TEM images of Se-NPs and Te-NPs displayed a spherical morphology, with the Te-NPs showing a clustered arrangement, which suggested electrostatic attraction among neighbouring particles. Particle hydrodynamic diameters (d H) measured with dynamic light scattering (DLS) further suggested monodisperse Se-NPs and polydisperse Te-NPs distributions, showing good agreement with AF4-MALS for Se-NPs, but suggests that the R g obtained from AF4-MALS for Te-NP was unreliable. The results demonstrate a complementary application of asymmetric flow field-flow fractionation (AF4), ICP-MS, light scattering, UV-Vis detection, and microscopic techniques to characterise biogenic Se and Te NPs.

Highlights

- Se and Te NPs were separated from liquid media using AF4
- PEGylation enables good recovery under high crossflow
- ICP-MS/MS enables detection of ultrasmall Te-NPs
- UV-Vis suggested detection of EPS alongside of NPs
- Improved sensitivity and lowered background signals from spICP-MS

Characterisation of selenium and tellurium nanoparticles produced by *Aureobasidium pullulans* using a multi-method approach.

Kenneth C Nwoko[a], Xinjin Liang[b], Magali AMJ Perez[a], Eva Krupp[a], Geoffrey Michael Gadd[b,d], Jörg Feldmann[a,c]

[a.] Trace Element Speciation Laboratories, Dept. of Chemistry, University of Aberdeen, AB24 3UE, United Kingdom

[b.] Geomicrobiology Group, School of Life Sciences, University of Dundee, Dundee, DD1 5EH, United Kingdom

[c.] Institute of Chemistry, Environmental Analytical Chemistry, University of Graz, 8010 Graz, Austria

[d.] State Key Laboratory of Heavy Oil Processing, State Key Laboratory of Petroleum Pollution Control, College of Science and Environment, China University of Petroleum, Beijing, 102249, China

Abstract: *Aureobasidium pullulans* was grown in liquid culture media amended with selenite and tellurite and selenium (Se) and tellurium (Te) nanoparticles (NPs) were recovered after 30 d incubation. A separation method was applied to recover and characterise Se and Te NPs by asymmetric flow field flow fractionation (AF4) with online coupling to multi-angle light scattering (MALS), ultraviolet visible spectroscopy (UV-Vis), and inductively coupled plasma mass spectrometry (ICP-MS) detectors. Additional characterisation data was obtained from transmission electron microscopy (TEM), and dynamic light scattering (DLS). Solutions of 0.2% Novachem surfactant and 10 mM phosphate buffer were compared as mobile phases to investigate optimal AF4 separation and particle recovery using Se-NP as a model sample. 88 % recovery was reported for 0.2 % Novachem solution, compared with 50 % recovery for phosphate buffer. Different Crossflow (C_{flow}) rates were compared to further investigate optimum separation, with recoveries of 88% and 30% for Se-NPs, and 90% and 29% for Te-NPs for 3.5 mL min^{-1} and 2.5 mL min^{-1} respectively. Zeta-potential (ZP) data suggested higher stability for NP elution in Novachem solution, with increased stability attributed to minimised NP-membrane interaction due to PEGylation. Detection with MALS showed monodisperse Se-NPs (45-90 nm) and polydisperse Te-NPs (5-65 nm).Single particle ICP-MS showed mean particle diameters of 49.7±2.7 nm, and 135 ± 4.3 nm, and limit of size detection (LOSD) of 20 nm and 45 nm for Se-NPs and Te-NPs respectively. TEM images of Se-NPs and Te-NPs displayed a

spherical morphology, with the Te-NPs showing a clustered arrangement, which suggested electrostatic attraction among neighbouring particles. Particle hydrodynamic diameters (d_H) measured with dynamic light scattering (DLS) further suggested monodisperse Se-NPs and polydisperse Te-NPs distributions, showing good agreement with AF4-MALS for Se-NPs, but suggests that the R_g obtained from AF4-MALS for Te-NP was unreliable. The results demonstrate a complementary application of asymmetric flow field-flow fractionation (AF4), ICP-MS, light scattering, UV-Vis detection, and microscopic techniques to characterise biogenic Se and Te NPs.

Keywords: Biogenic nanoparticles, selenium, tellurium, AF4, ICP-MS/MS, spICP-MS

1. Introduction

Selenium (Se) and tellurium (Te) are metalloid elements that belong to the chalcogen group in Group 16 of the Periodic table. Neither selenium or tellurium are extracted as primary ores; but are recovered as by-products during the processing of base metal ores such as Cu, Pb, Bi, Fe and other metals [1]. They have an extremely low crustal abundance (Se 0.05 – 0.09 mg kg^{-1}, Te 0.02 mg kg^{-1}) and have been classified among the 'critical' elements due to a potential risk in their security of supply [2-4] . Both selenium and tellurium are of economic interest because of their applications in advanced technologies such as photovoltaic cells for solar energy, and thin film technologies[5-7] . To improve their supply, new methods of extraction have been investigated including chemical reduction[8, 9], electrochemical processes[10, 11], and microbial biorecovery[12-14] . Microbial biorecovery of Se and Te in their elemental forms may offer an environmentally sustainable, relatively low-cost method for their production at but can be challenged by the low yield and tedious purification steps to obtain sufficient amounts.[15-18]. Various species of bacteria and fungi have been investigated for the intracellular and extracellular biosynthesis of Se and Te NPs, as a means to biotransform oxyanions of both elements to less toxic forms; and their exploitation in environmental, industrial and medical applications [15-18]. Se and Te NPs biosynthesised by fungi and bacteria have shown average diameters of 60-80 nm and 221 nm respectively , and may be associated with lipid, carbohydrate and/or protein on the surface of the produced Se and Te NPs [18, 19]. Prior to any potential industrial application, there is a need to characterise biosynthesised NPs to determine their size, composition, distribution, and dispersibility. Various established kinds of metrological techniques are already in use for NP characterisation based on their

quantification, separation and characterisation with each technique providing a specific kind of information[20]. In this study, separation of the NPs was achieved with asymmetric flow field-flow fractionation (AF4), an analytical technique which sequentially separates NPs in a thin channel in order of increasing particle size under the influence of a perpendicular crossflow[21-24] . One advantage of the AF4 technique is its versatility to be simultaneously coupled with multiple detectors, with multi-angle light scattering (MALS) and inductively coupled plasma mass spectrometry (ICP-MS) detectors providing particle size data and element-specific detection, respectively and able to detect nano- and microparticles in the same run. For single particle inductively coupled plasma mass spectrometry (spICP-MS), sufficiently diluted suspensions are detected above a background signal and counted in fast time resolved analysis (TRA) mode using ultrafast integration times[25, 26] . The introduction of a single NP into the plasma generates a packet of ions creating a pulse signal when it reaches the detector. The detector pulse is correlated to the total mass per particle and subsequently correlated to the particle size[27-30] .

The main advantages of spICP-MS are that it employs the power of an ICP plasma to completely destroy any biological matrix material; it uses very small sample volumes with sufficient dilution to ensure high sensitivity of signals above background and avoid detection of two particles in one measurement event. In this study, we demonstrated the need for complementary analytical techniques to characterise biogenic nanoparticles. In addition to the coupled AF4-UV-MALS-ICP-MS and spICP-MS analytical tools, the conventional and relatively straightforward techniques such as transmission electron microscopy (TEM) and dynamic light scattering (DLS) were employed to provide an enhanced analytical perspective for a better characterisation of biogenic Se/Te-NPs produced by the polymorphic fungus *Aureobasidium pullulans* when exposed to selenite and tellurite. Many fungi are capable of the reductive transformation of metalloid oxyanions, including Se and Te, to elemental forms which provides a biological system applicable to bioremediation and/or element biorecovery[13, 31].

2. Materials and Methods

2.1 Experimental

2.1.1 Biosynthesis of NPs by *A. pullulans*. Se and Te NPs biosynthesis by A. pullulans was performed following the protocol described by Liang *et al* [18] All reagents and chemicals used

were of analytical grade or better with all volumes measured gravimetrically. Liquid cultures were prepared in 250-mL Erlenmeyer conical flasks containing 100 mL nutrient medium on an orbital shaking incubator (Infors Multitron Standard, Rittergasse, Switzerland) at 125 rpm, 25°C in the dark. AP1 agar medium was used as the growth medium with previously stated nutrient consisting of (L^{-1} Milli-Q water): D-glucose 30 g, $(NH_4)_2SO_4$ 5 g, KH_2PO_4 0.5 g, $MgSO_4 \cdot 7H_2O$ 0.2 g, $CaCl_2 \cdot 6H_2O$ 0.05 g, NaCl 0.1 g, $FeCl_3 \cdot 6H_2O$ 0.0025 g, and trace metals: $ZnSO_4 \cdot 7H_2O$ 0.004 g, $MnSO_4 \cdot 4H_2O$ 0.004 g, $CuSO_4 \cdot 5H_2O$ 0.0004 g. All chemicals, apart from D-glucose, were prepared as 1 M stock solutions and autoclaved separately (121 °C, 15 min) before appropriately combining the required volumes to reach the desired final concentrations for AP1 liquid medium. Sodium selenite (Na_2SeO_3) or sodium tellurite (Na_2TeO_3) were dissolved separately in Milli-Q water and sterilized by membrane filtration with 0.2 µm cellulose nitrate filter paper (Whatman, Maidstone, Kent, UK) and added to autoclaved AP1 medium (121^{o}C, 15 min) at room temperature to give a final concentration of 1 mM. After autoclaving, the pH of liquid medium was adjusted to pH 5 using sterile 1 M HCl. *A. pullulans* was grown on AP1 agar medium for 4 d at 25°C prior to liquid subculture. For inoculation, ten 6 mm diameter inoculum plugs were taken from the margins of actively growing colonies using sterile cork borers (autoclaved at 121°C, 15 min) and added to 100 ml AP1 medium for incubation as described above. The ability of *A. pullulans* to reduce selenite and tellurite was assessed visually, the red (Se) or black (Te) colouration being used as an indicator of reduction to their elemental forms. The culture media was filtered through cellulose nitrate membrane filters (0.45 µm pore diameter, Whatman, Maidstone, Kent, UK) to obtain suspensions free of micro-sized particles. Particles present in the fungal supernatant were harvested by centrifugation at a series of speeds (4k, 8k and 13k x g), each centrifugation step lasting 30 min until the particles in the supernatant were separated from the biomass. Harvested particles were rinsed through a graded ethanol series (50-100%(v/vaq), 15 min per step), then rinsed three times with a 20 % (w/v) sodium dodecyl sulphate (SDS) solution and finally rinsed three times with autoclaved Milli-Q water (120 °C, 15 min) to remove remaining impurities.

2.1.2 Determination of total elemental Se/Te: 50 mg of the recovered suspensions was weighed into 50 mL sample vials, 4 mL aqua regia added, pre-digested overnight in a fume hood and subsequently digested in a microwave (Mars5, CEM Microwave Technology Ltd,

Buckingham, UK) using the open vessel method[32] . Trace element calibration standards (VWR, USA) in the range 1 µg L^{-1} to 100 µg L^{-1} were prepared and analysed for quantification of Se/Te by external calibration with inline addition of 10 µg L^{-1} Ge was used as an internal standard to monitor plasma fluctuation and cancel out sensitivity shifts. All analysis was performed in triplicate and errors reported as standard deviation.

2.1.3 Preparation of AF4 carrier solutions. AF4 carrier solutions were prepared fresh daily before measurement with de-ionised water (18.2 Ω cm) obtained from a Millipore system. Novachem surfactant (Postnova Analytics Landsberg, Germany) was diluted with de-ionised water in a 1000 mL volumetric flask to reach a concentration of 0.2% v/v. The Novachem surfactant is a mixture of cationic and anionic surfactants as follows (in wt.%): water 88.8, triethanolamine oleate 3.8, sodium carbonate 2.7, alcohols + C12-14-secondary ethoxylate 1.8, tetrasodium ethylenediaminetetraacetate 1.4, polyethylene glycol 0.9, sodium oleate 0.5, sodium bicarbonate 0.1. 10 mM phosphate buffer was prepared by dissolving 8 g of NaCl, 200 mg KCl, 240 mg KH_2PO_4, and 1.44 g Na_2HPO_4, in 800 mL of deionised water. The pH was adjusted to 7.4 with aqueous ammonia and deionised water added to a final volume of 1000 mL. Both solutions were stirred for 10 min and vacuum filtered through a 0.45 µm cellulose acetate filter.

2.1.4 Sample preparation for spICP-MS. 0.5 mL samples were transferred to 1.5 mL Eppendorf vials fitted with 10 kDa cut-off mesh. Vials were centrifuged at 10,000 x *g* for 3 min, the supernatant was discharged, and the pellets rinsed with 0.5 mL deionised water. The process was repeated, and the final pellet was resuspended in 0.5 mL deionised water, then transferred to 15 mL plastic tubes. Filtered samples were diluted with deionised ultrapure water prior to spICP-MS analysis. Transport efficiency was determined with measurement of a 50 mg kg^{-1} AuNP colloidal suspension (Nanocomposix, USA) with a nominal diameter of 60 nm as a reference standard since Se or Te nanoparticle certified reference standards are not currently available. The Au-NP suspension was diluted by a factor of 10^{-6} to give a final concentration of 50 ng kg^{-1}. Elemental aqueous standards of Se and Te of 1 µg L^{-1} were prepared for the determination of elemental response factors. All samples were bath sonicated at 37 kHz for 10 min before analysis.

2.2 Instrumental analysis

2.2.1 AF4-UV-MALS. AF4 analysis was performed with a metal-free AF 2000 system (Postnova Analytics, Landsberg, Germany), with inbuilt software for data acquisition. The separation system consisted of a solvent degasser, solvent organiser, two isocratic solvent pumps, a pair of Kloehn pumps for generation of the crossflow, an auto-sampler, and a separation channel. The separation channel consisted of a trapezoid cartridge, fitted with a spacer of 350 μm nominal height and a regenerated cellulose acetate membrane with molecular weight cut-off (MWCO) of 10 kDa as the accumulation wall. The auto-sampler and oven temperatures were maintained at 4 ^{o}C and 20 °C, respectively. The AF4 system was coupled to UV-Vis, multi-angle light scattering (MALS) detectors and an ICP-MS through an interface system. The MALS detector consisted of 21 light scattering cells at angles between 7^{o} and 164^{o}, with a laser light intensity of 50 mW and wavelength of 532 nm. A sample volume of 20 μL was maintained throughout, with at least triplicate injections per sample. Sample carryover was eliminated by injecting 1 % HNO_3 solution for 5 min after each run to flush the AF4 channel.

2.2.2 ICP-MS/MS: ICP-MS/MS analysis was performed using an Agilent 8800 ICP-MS/MS (Agilent Technologies, Santa Clara, USA) instrument. The ICP-MS instrument was fitted with a Micromist nebulizer and a Scott double pass spray chamber. ICP-MS/MS operating conditions are listed in Table S1.

2.2.3 spICP-MS: Single particle ICP-MS analysis was performed using an Agilent 7900 ICP-MS equipped with a Micromist nebulizer, double pass spray chamber and an autosampler. The system was fitted with a quartz torch with internal diameter of 1 mm to reduce signal background and improve sensitivity. Nanoparticle diameters for all the samples were reported as an average diameter of six replicates. Collision cells were pressurised with 3.5 mL min^{-1} H_2 gas in both ICP-MS/MS and sp-ICP-MS measurements to remove interfering species. Instrumental parameters (lens position, torch position) were optimised daily to achieve maximum sensitivity with an aqueous tune solution of 10 µg L^{-1} Li, Co, Y, Ce, Tl. Data analysis was performed using Agilent MassHunter 4.4 software (Agilent Technologies, USA).

2.2.4 TEM: Samples were bath sonicated at 37 kHz for 5 min and 5 μL aliquots transferred using a micropipette onto a Formvar-coated 200-mesh copper grid and left to dry in ambient conditions for 20 min. TEM Images were acquired with a JEOL-1400 plus electron microscope, at an accelerating voltage of 80 kV, using an AMT UltraVUE camera. After image acquisition,

they were filtered, and individual points were counted as NPs using ImageJ processing software, assuming a spherical morphology for the NPs; particle diameters were calculated from areas of individual spheres.

2.2.5 Dynamic light scattering (DLS): DLS analysis in batch mode was performed with a Malvern Zetasizer Nano ZS (Malvern Panalytical, Worcestershire, UK) system with a He-Ne laser as the light source at 632 nm and 173° scattering angle. Samples were dispersed in deionised water with refractive index (1.33), viscosity (8.9×10^{-4} Pa s) and temperature (25°C) inputted into the measurement file. The sample suspensions were diluted 1:100 *v/v* with deionised water followed by 120 s equilibration time. Average particle sizes based on scattered light intensity weighted averages were automatically calculated by the software based on the Stokes-Einstein theory and reported as hydrodynamic diameters. The instrument also enabled the determination of the zeta-potential under same instrumental settings with equilibration time of 120 s. The determination of the zeta-potential was based on the Smoluchowski model with a Henry's Function F(Ka) of 1.5.

3. Results and Discussion

3.1 Total biogenic SeNPs and TeNPs generated by *A. pullulans*

After 30-day incubation, nanoparticles were harvested from supernatants of *A. pullulans* after growth in AP1 medium amended with 1 mM Na_2SeO_3 (79 mg Se L^{-1})/Na_2TeO_3 (128 mg Te L^{-1}). Total yields of SeNPs and TeNPs harvested from the supernatant were 81.6 ± 1.4 mg L^{-1}, 21.5 ± 0.1 mg L^{-1} (*n=3*) respectively. Previous research has already demonstrated that SeNPs and TeNPs can be located both intracellularly and extracellularly[18, 33]this work focused on the extracellular SeNPs and TeNPs harvested from the fungal supernatant because of their relative ease of separation from the biomass and media. It appeared that the biotransformation of selenite to elemental selenium was quantitative while the biotransformation from tellurite to elemental tellurium saw only resulted in a conversion of 16.8%. Se and Te species can betoxic to microbes, with Te reported to show higher toxicity at lower concentrations than Se [34]. In some microbes, Te-oxyanions such as tellurite react with thiols such as glutathione (GSH); which supports the conversion of tellurite to elemental tellurium [35]. The low yield of Te-NPs by *A.pullulans* is therefore suggested to be linked to Te toxicity which though is not fully understood in fungi, could be caused by the accumulation

of reactive oxygen species (ROS) as a result of depletion of GSH and resultant loss of anti-oxidant capability.

3.2 **AF4 method development and optimisation**

From field-flow fractionation (FFF) theory, retention time (t_r) is directly proportional to particle size and is dependent on parameters such as absolute temperature, area of the accumulation wall, crossflow rate, viscosity of the mobile phase, channel flow, and channel thickness[21, 22] . A combination of AF4 parameters such as membrane type, crossflow rate (C_{flow}), focus flow rate, channel thickness, ionic strength of carrier, and sample load have been established to influence optimum separation and recovery in the AF4 technique to various degrees[36, 37] . In our study, AF4 separation parameters of mobile carrier and C_{flow} rates were investigated for their influence on recovery and elution of the Se/Te-NPs. The 0.2% v/v Novachem solution was compared with a buffer solution, (10 mM phosphate buffer, pH=7.4), to compare their suitability as an AF4 mobile carrier for the microbial sample matrices. Recoveries obtained from UV-Vis signals (Figure 1) were compared with the peak area of an injection without a C_{flow}, using the formula (Equ. 1) [38] :

$$R\ (\%) = A/A_0 \times 100 \qquad \text{Equ. 1}$$

where, A= Peak area obtained with a crossflow
A_0= Peak area without an applied crossflow

Recoveries of 88% and 50% were recorded for the Se-NPs using 0.2% v/v Novachem solution and 10 mM phosphate buffer, respectively. Both 0.2% v/v Novachem solution and 10 mM phosphate buffer influenced the analyte retention times; the Se-NP peak was observed at 26 min in 0.2% v/v Novachem solution, and 30 min in phosphate buffer. This indicated that the surface of SeNPs were modified with phosphate buffer which could be due to an electrostatic effect, such that the SeNPs have lower surface charges resulting in a higher level of membrane adsorption and consequently elute later. The electrostatic effect might also be related to the ζ-potential (ZP) of the NPs (Table 1). A net negative surface ZP has been reported for the 10 kDa membrane in past studies [39, 40]. Theoretically, lower ZP values might indicate lower stability and promote aggregation/adhesion, while higher ZP values would indicate better stability [41]. The phosphate ions would be expected to impart a negative charge to the Se-NPs which would enhance repulsion between the membrane and surface NPs, but this

appears not to be the case, as attractive forces appear to be present. Also, the higher ionic strength may also increase the compression of the electric double layer (EDL) and decrease ZP [42]. Furthermore, it appears that polyethylene glycol (PEG) in the Novachem surfactant facilitates the formation of a PEGylated corona around the NP which increases its stability [43]and may minimize interaction with the membrane which consequently improves recovery. Though maximum electrostatic repulsion determined by ZP measurements is required to ensure minimal contact between the NPs surface and the membrane, it is challenging to explain electrostatic attractive forces which may be present (such as Van der Waals forces). Therefore, ZP data must be interpreted and applied with caution. Also, accurate ZP measurements in cell culture medium are challenging because of their enrichment with ions which increases conductivity and interferes with ZP measurement [42].

Table 1 ZP values of Se-NP and Te-NP dispersed in AF4 running solutions

Figure 1. Representative AF4-MALS-UV fractograms depicting the effect of mobile phases using 0.2% v/v Novachem solution (NVC, red traces) in comparison with 10mM phosphate buffer (PO_4; black traces); as detected by light scattering (LS 90°) (top fractogram)and UV-Vis (bottom fractogram) at 280 nm wavelength. Novachem solution demonstrated faster elution and better analyte recovery (88%) than phosphate buffer (50%). Analysis conditions for AF4 are reported in Table S2 (Supplementary information).

To optimise the AF4 method, an elution programme with an optimal C_{flow} rate was investigated and sample recoveries monitored with the UV-Vis, MALS and ICP-MS/MS detectors with recovery calculations shown with ICP-MS/MS signals (Figure 2). A 2 mL min^{-1} C_{flow} resulted to a narrow Se peak at 17 min (30% recovery), compared to the 88% recovery rate with a C_{flow} of 3.5 mL min^{-1}, with a symmetrical monodisperse peak. Similarly, TeNPs eluted with C_{flow} 3.5 mL min^{-1} also showed a larger peak area with higher recovery (90%) compared to Te-NPs eluted at 2 mL min^{-1} with low recovery (29%). Separation with a 3.5 mL min^{-1} crossflow, showed larger peak areas and consequently better analyte recoveries with

clearer separation of peaks. C_{flow} rate is a critical AF4 separation parameter [44, 45]. Though it is expected from FFF theory that a higher crossflow increases the chances of membrane adhesion and poor recovery [46], previous studies have reported that the filtration of complex samples prior to injection improves analyte recovery [39]. It appears that filtration through a 0.45 µm cellulose acetate filter significantly reduced the amount of biological debris and micro-sized particles in the sample matrix which would otherwise adhere to the membrane. Another possible explanation for this observation is that the higher repulsion generated between the negatively charged Se-NP and the negative ZP of the membrane causes the particle to diffuse faster, hence shorter time and also higher recovery.

Figure 2. AF4-ICP-MS/MS fractograms depicting the comparison of different C_{flow} rates on the recovery of Se-NP (red traces) and Te-NP (black traces using 0.2% v/v Novachem solution as mobile phase. C_{flow} rates of 3.5 mL min^{-1} (bottom fractogram, B) for both Se-NP and Te-NP indicated higher analyte recovery compared with C_{flow} of 2.0 mL min^{-1}. Analytical conditions for ICP-MS/MS are reported in Table S1 (Supplementary information).

The C_{flow} programme in exponential decay mode applied in this study consumed more carrier liquid compared to a linear-mode, but it provided a better separation resolution, recovery, and sensitivity for aggregated samples. It also has been validated in the AF4 separation of pullulan and hydroxypropyl cellulose by Leeman *et al* [47] . Moreover, the Se-NP peak appeared towards the end of the applied C_{flow} in the elution programme, suggesting that the Se-NPs have a reversible, strong attractive force towards the membrane in contrast to the Te-NPs which completely eluted within the elution timeframe with an applied C_{flow}.

3.3 **Particle sizing by AF4-MALS**

Radii of gyration were computed from MALS signals based on a spherical fit model and showed good data fit across the light scattering angles (Figure S1). The MALS detector was calibrated using 5 mg/mL bovine serum albumin (BSA) and 0.2% Novachem solution as eluent as recommended by the instrument manufacturer's protocol (Postnova Analytics GmbH). A

molar weight of 66,000 g/mol was recorded for BSA with the application of 0.185 mL/g for refractive index increment (dn/dc) while the second virial coefficient was considered negligible considering the very dilute concentrations typical of AF4 separations [48].

Se-NPs showed a particle size range of 45 nm – 90 nm with a mean R_g value of 80.0 nm and appeared monodisperse; while Te-NPs showed a mean R_g of 29.5 nm, within a range of 5 nm to 65 nm and were polydisperse. The Te-NP ICP-MS/MS traces (Figure 2) clearly highlighted the detection of three fractions of Te-NPs between 4 min (t_0) and 15 min, which are not visible from the MALS trace (Figure. 3B), demonstrating the higher sensitivity and specificity of ICP-MS/MS over MALS detection. Furthermore, intense UV-Vis signals for both elements suggested the detection of light absorbing biomolecules in the NPs, which have been previously reported to be extracellular polymeric substances (EPS) secreted by *A. pulluans*[18] The UV-Vis- and MALS peaks for Se-NPs (Figure S3) appeared to be well-overlaid suggesting that the EPS surrounded the Se-NPs surface. However, the UV-Vis peak however shows a peak at around 20 min without a corresponding MALS signal, which suggests a different biomolecule present in the EPS which is not bound to the NP. For the Te-NPs, the UV-Vis signal showed two peaks between 20 min and 25 min which also suggested the presence of multiple biomolecules present in the EPS. The MALS signal was detected at 30 min,suggesting the detection of large sized non-Te containing NP, while the fraction of EPS detected with UV-Vis (20-25 min) showed the absence of light scattering molecules. It can be inferred that the Te-NPs were unstable and disintegrate in the channel during separation. Also, Te-NPs below 100 nm have been reported to exhibit plasmonic-like scattering like Au-NPs[49]and in this case appeared to interfere with the light scattering signal which may explain the near absent MALS signal between 4 and 15 min.

Figure 3. AF4-MALS fractograms of Se-NPs (top fractogram, A) and Te-NPs (bottom fractogram, B) detected by light scattering ((LS 90°) on the left axis, and radius of gyration (R_g) on the right axis, with size computation based on a spherical fit model. Demonstration of data fit across light scattering angles is depicted in Figure S1 (Supplementary information). Se-NPs showed a narrow monodisperse structure with a range of 45-90 nm, while Te-NPs were polydisperse with a 5-65 nm.

3.4 **Single particle ICP-MS**

In single particle ICP-MS (spICP-MS), particle diameter is dependent on the total mass introduced into the plasma through the nebulizer (transport efficiency), which in this study was calibrated against a 50 ng kg^{-1} Au-NP (60 ± 5 nm) certified reference material following the protocol reported in our previous work[50] . The spICP-MS results showed a median particle diameter 49.7±2.7 nm for Se-NPs, and a limit of size detection (LOSD) of 20 nm, attributed to reduced background signal levels. This reduced background signal arose from a number of factors: measurement of the more abundant ^{78}Se isotope and removal of argon dimer (^{40}Ar ^{38}Ar) interference resulting from the addition of H_2 gas to the collision cell[51]; and the ultracentrifugation of the samples with a 10 kDa cut-off filter during sample preparation which removed excess dissolved Se/Te from the samples and consequently reduced the background.

Figure 4. Time scans and particle size-frequency distribution of NP signals acquired for Se(A), and Te(B) at a dwell time of 0.1 ms. MassHunter software analysis indicated a median diameter of 49.7±2.7 nm Se-NPs, and 135±0.3 nm Te-NPs. Limits of size detection (LOSD) were 20 nm, and 45 nm for Se-NP and Te-NP, respectively. Analytical conditions for sp-ICP-MS are reported in Table S1 (Supplementary information).

The Te-NPs showed a median diameter of 135 ± 0.3 nm and are therefore significantly larger than the SeNPs. However, the particle-size distribution (PSD) is not normally distributed because the measurement of a NP suspension with spICP-MS always produces a combined signal containing both dissolved ions and particles. Thus, in calculating the PSD frequencies of a NP suspension, the instrumental software assumes that the lowest intensities in the histogram arose from particle free measurements. However, the dissolved analyte signal actually contributes to the determination of the PSD, despite of the apparent removal of dissolved analyte signal from the data during PSD calculations[52] . This is responsible for the LOSD of 45 nm for Te-NPs, which was an improvement from the LOSD of 80 nm for biogenic Te-NPs reported by Gómez-Gómez *et al.* [53]. Like in the case of the Se-NP, this also appeared to be related to the removal of excess dissolved tellurium using the ultracentrifugation cut-off membrane and subsequent dilution of the samples. However, one disadvantage of the ultracentrifugation step could be the loss of smaller sized NPs, which may cause a bias in particle counting in favour of larger sized particles as seen with the Te-NPs. In addition, enhanced particle detection and counting was achieved in this study with a 0.1 ms dwell time

compared with a 3 ms dwell time reported in the study by Gómez-Gómez [53] . Mean R_g (80 nm) from AF4-MALS correlated with the median diameters (49.7 nm) recorded by spICP-MS for Se-NPs (which represents only Se, assuming a core of only Se). AF4-MALS R_g values suggested a corona surrounding the Se-NP, which was likely to be secreted extracellular protein from the fungi which behave as capping agents[54] .

3.5 **TEM**

Microscopic examination is a conventional, fast, direct, and simple technique to examine NP morphology and determine core particle diameters (as equivalent circular diameters) by counting the number of representative particles as originally reported by Woehrle *et al*[55] . TEM images indicated spherical morphologies for both NPs, but the Te-NPs were arranged in clusters or aggregates while the Se-NPs were randomly distributed (Figure. 5).

Figure 5. TEM images (top left and bottom left) and frequency size graphical distributions (top right and bottom right) of Se-NPs (A) and Te-NPs (B). Se-NPs displayed spherical shapes and randomly distributed, while Te-NPs displayed a clustered arrangement.

The formation of clusters can be attributed to electrostatic interactions from functional groups present in the proteins and polysaccharides contained in the extracellular polymeric substances (EPS) which have been associated with biogenic tellurium recovered from fungal biomass [14] . The TEM average particle diameters for Se-NP (35.5±2.5 nm) were comparable with spICP-MS (49.7±2.7 nm) and reflected a more realistic particle size since the NPs measured with TEM did not undergo additional sample preparatory steps such as dilution and centrifugation which might alter particle size. TEM also captures smaller sized particles below the particle LOSD recorded with spICP-MS (10 nm for Se-NP, 15 nm for Te-NP) which makes it an attractive technique for measurement of ultrasmall NPs. However, TEM measures only a small proportion of the sample and therefore assesses fewer number of particles compared to AF4 and spICP-MS.

3.6 **Particle sizing by dynamic light scattering (DLS)**

DLS provides a quick non-invasive, non-specific technique to obtain particle size distributions (as hydrodynamic diameters, d_H) and polydispersity index of colloids in solution. DLS theory

is based on correlating the light scattered by particles and undergoing Brownian motion, to their size and shape based on the Stokes-Einstein equation[56]. Irradiation of colloidal particles dispersed in a liquid medium by a laser source causes changes in light intensity over time; these changes are related to the particle diffusion coefficient. Bigger particles diffuse slowly causing changes in the intensity of scattered light over a larger time scale, while the smaller particles move faster. Therefore, an ideal solution for DLS must be sufficiently diluted and free of large particles that can cause interference. To minimise multiple scattering and interference from artefacts such as dust, the DLS instrument was equipped with non-invasive backscattering (NIBS) which detects scattered light at a 173° angle[57, 58] . Quality control of DLS data was ensured by measuring latex particles (diluted in water), showing diameters of 64 ± 2.6 nm and 131 ± 2.5 nm which were within range of certified values (60 ± 3 nm, and 125± 2 nm) respectively. Samples were measured at least in triplicates at least and showed good reproducibility of peaks for Se-NPs, while in Te-NPs, the overlaid peaks suggested non-uniform scattering that may be caused by the presence of aggregates. A polydispersity index (PDI) below 0.7 suggests a monodisperse NP distribution while values above 0.7 are considered polydisperse[59] . Se-NPs showed a monodisperse distribution (Figure 6) with a polydispersity index of 0.2, while Te-NPs showed a polydispersity index of 0.7 and were therefore considered more polydisperse. Since both AF4-MALS and DLS provide the particle size as an ensemble, both techniques can therefore be directly compared. This can also be attributed to calculation methodologies used for both DLS and MALS which work well for monodisperse samples but are not always appropriate for polydisperse samples[60] ..

Figure 6. DLS fractograms showing intensity weighted distributions for Se-NPs (A) and Te-NPs (B) at the top half of the panel and overlay of triplicate analysis of Se-NPs (C) and Te-NPs (D). Average diameters of 167±1.4 nm and 174 ± 2.1 nm were recorded for Se-NPs and Te-NPs.

A summary of the particle radii obtained from the different techniques reflected the different principles of each technique (Table 2). Theoretically, DLS and AF4-MALS measure the size of the particle core and any surrounding material including the surface coating which may be contributed by stabilizing agents. spICP-MS measures the size distribution of the inorganic NP

particle core from its elemental mass, while TEM is a non-specific technique which applies transmitted electrons which enables the visualisation and counting of the "particles" on the sample grid, which may sometimes include particle aggregates. Therefore, particle sizes obtained from DLS cannot be accurately compared with spICP-MS because DLS is very non-specific and measures hydrodynamic diameter while spICP-MS measures the diameter of a single spherical particle and is element specific, i.e., it reports the size of the Se or Te core of the Se-NP and Te-NP, respectively. DLS must therefore be considered only as a screening approach to investigate the presence or absence of submicron particles regardless of their chemical composition.

For Se-NPs, Table 2 showed that the mathematical radius detected with spICP-MS was 1/3 of the hydrodynamic radius (R_H) detected with AF4-MALS and DLS, with the latter two techniques showing good agreement (Table 2). The AF4-MALS and DLS data can be possibly attributed to a corona surrounding the Se-NP core comprising a solvent hydration layer, adsorbed salts on the NP surface, and extracellular polymeric substances (EPS) secreted by *A. pullulans* [61, 62]; with an assumption that the particle has a pure elemental selenium core. The particle sizes of the Se-NP measured with spICP-MS and TEM are comparable considering that the spICP-MS average particle radius of 25 nm was close to its limit of size detection (LOSD) of 20 nm reported for Se-NPs. The TEM images of Se-NPs also appeared randomly distributed suggesting some overlap between smaller and larger sized particles, which makes it challenging for the ImageJ software to assign an accurate average particle size.

The Te-NPs showed a distinct difference from the Se-NPs. Particle radii from DLS were far higher than AF4-MALS and may suggest non-uniform light scattering caused by the presence of aggregates in the sample. Excessive aggregation detected by the DLS technique for Te-NPs compared to Se-NPs is evident from their standard deviation values (±3.1 vs ±0.9). The AF4-ICP-MS/MS and AF4-MALS fractograms (Figure 2B and 3B) also suggested a highly aggregated and polydisperse sample distribution with 4 Te-NPs size fractions which were more clearly detected by AF4-ICP-MS/MS (Figure 2B). AF4-MALS (Figure 3B) and AF4-UV (Figure S3) peaks were observed between 20 and 30 min but were undetected with AF4-ICP-MS/MS (Figure 2B) which strongly suggested the presence of biomolecules or EPS which have detached from the Te-NP surface.

Furthermore, the ultra-small sized TeNPs detected at the beginning of the AF4-ICP-MS/MS and AF-MALS fractograms might induce a high surface free energy that accelerated the

aggregation of adjacent Te-NPs, which resulted in unreliable particle data when light scattering techniques (AF4) were applied. Moreover, the relative less dense surface coating of the Te-NPs might cause the numerous unsaturated coordination sites on the NP surface to easily absorb or bond with the solvent molecules[63] . It is also possible that the aggregated NPs became unstable and broke down in the AF4 channel, as reported for mercury NPs by Ruhland *et al*. [64]. spICP-MS measures the aggregates as one whole particle without breaking them up resulting in an apparent larger average particle radius (67 nm) ; with the highest standard deviation (±4.3) amongst the 4 techniques further suggesting that the Te-NPs were heterogeneously distributed and more polydisperse than the Se-NPs. The TEM images showed a tightly clustered distribution which further indicated that the Te-NPs tend to form aggregates. The TEM average particle radius of 19.5 nm further supports the observation of a tightly clustered distribution which might be a result of strong electrostatic interaction between the Te-NPs and the surrounding medium.

Table 2. Summary of particle sizes measured with the different techniques. Errors are given as standard deviation of triplicates; diameters and mathematical radius are shown (in parentheses).

4. Conclusions

Selenium and tellurium nanoparticles were harvested from *A. pullulans* grown in liquid medium amended with sodium selenite and sodium tellurite for 30 days and characterised using different techniques. Based on the results presented in this work, the NPs have been separated with field-flow fractionation and characterised (particle size, shape, morphology, and distribution) with mass spectrometry and optical techniques. Various flow and sample parameters influence an optimal AF4 separation, and therefore a minimal number of parameters should be identified during an analytical study to conserve time and resources. The major advantage of AF4 fractionation is its capability to be simultaneously coupled with multiple detectors to achieve high resolution NP separation from a complex matrix, particle concentration, size distribution, elemental detection in one single run. The coupling of AF4-MALS-UV with spICP-MS analysis for inorganic nanoparticle detection has been reported [65, 66], an inability to couple both techniques was therefore considered to be a major limitation of this study. To achieve optimal separation with asymmetric flow field-flow fractionation

(AF4), a surfactant-based carrier solution and a high crossflow were applied which showed particularly good recoveries and resolution. Based on their elution behaviour, Se-NPs and Te-NPs displayed different particle physico-chemical properties and flow behaviour in the AF4 channel. ICP-MS showed high sensitivity over MALS particularly with the detection of ultrasmall Te-NPs. Particle diameters obtained from spICP-MS suggested either a bias in favour of the counting of larger sized particles, or aggregation especially for Te-NPs. Improvement in LOSD for Se and Te measured with spICP-MS demonstrated the reliability of our data and is an improvement on previous studies. Though TEM and DLS are non-specific and regarded as conventional and relatively easy techniques, they are strong tools to provide imaging and size distribution for NPs, requiring low sample volumes and providing easily interpretable data. As ensemble sizing techniques, DLS and MALS data showed good agreement for a monodisperse Se-NP with dense polymer layer which was free of aggregates, while suggesting the detection of polydisperse Te-NP aggregates. The study has contributed further to understanding the nature of biogenic Se and Te NPs and their characterization and illustrated that a multi-method approach is necessary to characterise these natural NPs in a more holistic way.

Declaration of Conflicting Interests

None

Acknowledgements

KCN acknowledges the receipt of joint PhD research funding received from the University of Aberdeen's Elphinstone studentship award, and the Federal Government of Nigeria through the Niger-Delta Development Commission (NDDC) Foreign Postgraduate Scholarship Scheme. JF and KCN gratefully acknowledge Postnova Analytics, UK for loaning of the AF4 system and technical support, and the Microscopy and Histology Facility at the Institute of Medical Sciences, University of Aberdeen for TEM measurements. G.M.G. gratefully acknowledges research support from Natural Environment Research Council (NE/M010910/1) under the NERC Security of Supply of Mineral Resources Grant Programme: Tellurium and Selenium cycling and supply (TeaSe).

Authorship contribution statement

Kenneth C Nwoko: Writing-original draft, review and editing, sample preparation, instrumental analysis (AF4-UV-MALS-ICP-MS/MS), DLS, TEM.

Xinjin Liang: Growth and culture experiments, review, editing.

Magali AMJ Perez: Sample preparation and instrumental analysis (spICP-MS, TEM).

Eva Krupp: Supervision.

Geoffrey Michael Gadd: Conceptualization, supervision, funding acquisition, review, editing.

Jörg Feldmann: Conceptualization, supervision, funding acquisition, review, editing.

References

[1] M. Bouroushian, in Anonymous Chalcogens and Metal Chalcogenides. Electrochemistry of Metal Chalcogenides. Springer, 2010, p. 1-56.

[2] Z. Hu, S. Gao, Upper crustal abundances of trace elements: a revision and update, Chem. Geol. 253 (2008) 205-221.

[3] L.T. Peiró, G.V. Méndez, R.U. Ayres, Material flow analysis of scarce metals: Sources, functions, end-uses and aspects for future supply, Environ. Sci. Technol. 47 (2013) 2939-2947.

[4] S.C. Spinks, J. Parnell, D. Bellis, J. Still, Remobilization and mineralization of selenium–tellurium in metamorphosed red beds: evidence from the Munster Basin, Ireland, Ore Geology Reviews 72 (2016) 114-127.

[5] S. Davidsson, M. Höök, Material requirements and availability for multi-terawatt deployment of photovoltaics, Energy Policy 108 (2017) 574-582.

[6] A. Naumov, Selenium and tellurium: state of the markets, the crisis, and its consequences, Metallurgist 54 (2010) 197.

[7] S. Wang, Tellurium, its resourcefulness and recovery, JOM 63 (2011) 90.

[8] F. Zhang, Y. Zheng, G. Peng, Selection of reductants for extracting selenium and tellurium from degoldized solution of copper anode slimes, Transactions of Nonferrous Metals Society of China 27 (2017) 917-924.

[9] H. Pasdar, B. Hedayati Saghavaz, M. Masoumi, A simple method for the recovery of selenium from copper anode slime sample using alkaline roasting process, International Journal of New Chemistry 6 (2019) 143-150.

[10] Y. Wang, Y. Xue, J. Su, S. Zheng, H. Lei, W. Cai, W. Jin, Efficient electrochemical recovery of dilute selenium by cyclone electrowinning, Hydrometallurgy 179 (2018) 232-237.

[11] W. Jin, J. Su, S. Chen, P. Li, M.S. Moats, G. Maduraiveeran, H. Lei, Efficient electrochemical recovery of fine tellurium powder from hydrochloric acid media via mass transfer enhancement, Separation and Purification Technology 203 (2018) 117-123.

[12] A. Ramos-Ruiz, J.A. Field, J.V. Wilkening, R. Sierra-Alvarez, Recovery of elemental tellurium nanoparticles by the reduction of tellurium oxyanions in a methanogenic microbial consortium, Environ. Sci. Technol. 50 (2016) 1492-1500.

[13] X. Liang, M.A.M. Perez, S. Zhang, W. Song, J.G. Armstrong, L.A. Bullock, J. Feldmann, J. Parnell, L. Csetenyi, G.M. Gadd, Fungal transformation of selenium and tellurium located in a volcanogenic sulfide deposit, Environ. Microbiol.(2020) .

[14] J. Mal, Y.V. Nancharaiah, N. Maheshwari, E.D. van Hullebusch, P.N.L. Lens, Continuous removal and recovery of tellurium in an upflow anaerobic granular sludge bed reactor, Journal of Hazardous Materials 327 (2017) 79-88.

[15] R. Borghese, M. Brucale, G. Fortunato, M. Lanzi, A. Mezzi, F. Valle, M. Cavallini, D. Zannoni, Reprint of “Extracellular production of tellurium nanoparticles by the photosynthetic bacterium Rhodobacter capsulatus”, J. Hazard. Mater. 324 (2017) 31-38.

[16] E. Zonaro, E. Piacenza, A. Presentato, F. Monti, R. Dell’Anna, S. Lampis, G. Vallini, Ochrobactrum sp. MPV1 from a dump of roasted pyrites can be exploited as bacterial catalyst for the biogenesis of selenium and tellurium nanoparticles, Microbial cell factories 16 (2017) 1-17.

[17] E.J. Espinosa-Ortiz, E.R. Rene, F. Guyot, E.D. van Hullebusch, P.N.L. Lens, Biomineralization of tellurium and selenium-tellurium nanoparticles by the white-rot fungus Phanerochaete chrysosporium, Int. Biodeterior. Biodegrad. 124 (2017) 258-266.

[18] X. Liang, M.A.M. Perez, K.C. Nwoko, P. Egbers, J. Feldmann, L. Csetenyi, G.M. Gadd, Fungal formation of selenium and tellurium nanoparticles, Appl. Microbiol. Biotechnol. 103 (2019) 7241-7259.

[19] E. Zonaro, S. Lampis, R.J. Turner, S.J.S. Qazi, G. Vallini, Biogenic selenium and tellurium nanoparticles synthesized by environmental microbial isolates efficaciously inhibit bacterial planktonic cultures and biofilms, Frontiers in microbiology 6 (2015) 584.

[20] N.L. Pacioni, in Anonymous Metrology for Metal Nanoparticles. Handbook of Ecomaterials. Springer, 2018, p. 1-16.

[21] M.E. Schimpf, K. Caldwell, J.C. Giddings, Field-flow fractionation handbook. John Wiley & Sons, 2000, .

609 [22] H. Lee, S.K.R. Williams, J.C. Giddings, Particle size analysis of dilute environmental
610 colloids by flow field-flow fractionation using an opposed flow sample concentration
611 technique, Anal. Chem. 70 (1998) 2495-2503.

612 [23] J.C. Giddings, Field-flow fractionation: analysis of macromolecular, colloidal, and
613 particulate materials, Science 260 (1993) 1456-1465.

614 [24] P. Li, J.C. Giddings, Isolation and measurement of colloids in human plasma by
615 membrane-selective flow field-flow fractionation: Lipoproteins and pharmaceutical colloids,
616 J. Pharm. Sci. 85 (1996) 895-898.

617 [25] C. Degueldre, P. Favarger, S. Wold, Gold colloid analysis by inductively coupled plasma-
618 mass spectrometry in a single particle mode, Anal. Chim. Acta 555 (2006) 263-268.

619 [26] C. Degueldre, P. Favarger, Colloid analysis by single particle inductively coupled plasma-
620 mass spectroscopy: a feasibility study, Colloids Surf. Physicochem. Eng. Aspects 217 (2003)
621 137-142.

622 [27] W. Lee, W. Chan, Calibration of single-particle inductively coupled plasma-mass
623 spectrometry (SP-ICP-MS), J. Anal. At. Spectrom. 30 (2015) 1245-1254.

624 [28] G. Cornelis, M. Hassellöv, A signal deconvolution method to discriminate smaller
625 nanoparticles in single particle ICP-MS, J. Anal. At. Spectrom. 29 (2014) 134-144.

626 [29] F. Laborda, J. Jiménez-Lamana, E. Bolea, J.R. Castillo, Selective identification,
627 characterization and determination of dissolved silver (I) and silver nanoparticles based on
628 single particle detection by inductively coupled plasma mass spectrometry, J. Anal. At.
629 Spectrom. 26 (2011) 1362-1371.

630 [30] W. Haiss, N.T. Thanh, J. Aveyard, D.G. Fernig, Determination of size and concentration
631 of gold nanoparticles from UV− Vis spectra, Anal. Chem. 79 (2007) 4215-4221.

632 [31] X. Liang, G.M. Gadd, Metal and metalloid biorecovery using fungi, Microbial
633 biotechnology 10 (2017) 1199-1205.

634 [32] A. Raab, M. Stiboller, Z. Gajdosechova, J. Nelson, J. Feldmann, Element content and
635 daily intake from dietary supplements (nutraceuticals) based on algae, garlic, yeast fish and
636 krill oils—Should consumers be worried? Journal of Food Composition and Analysis 53
637 (2016) 49-60.

638 [33] F.G. Martínez, G. Moreno-Martin, M. Pescuma, Y. Madrid-Albarrán, F. Mozzi,
639 Biotransformation of selenium by lactic acid bacteria: formation of seleno-nanoparticles and
640 seleno-amino acids, Frontiers in Bioengineering and Biotechnology 8 (2020) 506.

641 [34] T.G. Chasteen, D.E. Fuentes, J.C. Tantaleán, C.C. Vásquez, Tellurite: history, oxidative
642 stress, and molecular mechanisms of resistance, FEMS Microbiol. Rev. 33 (2009) 820-832.

643 [35] R.J. Turner, Y. Aharonowitz, J.H. Weiner, D.E. Taylor, Glutathione is a target in tellurite
644 toxicity and is protected by tellurite resistance determinants in Escherichia coli, Can. J.
645 Microbiol. 47 (2001) 33-40.

646 [36] U.B. Kavurt, M. Marioli, W.T. Kok, D. Stamatialis, Membranes for separation of
647 biomacromolecules and bioparticles via flow field-flow fractionation, Journal of Chemical
648 Technology & Biotechnology 90 (2015) 11-18.

649 [37] H. Dou, E.C. Jung, S. Lee, Factors affecting measurement of channel thickness in
650 asymmetrical flow field-flow fractionation, Journal of Chromatography A 1393 (2015) 115-
651 121.

652 [38] B. Meisterjahn, S. Wagner, F. von der Kammer, D. Hennecke, T. Hofmann, Silver and
653 gold nanoparticle separation using asymmetrical flow-field flow fractionation: influence of
654 run conditions and of particle and membrane charges, Journal of Chromatography A 1440
655 (2016) 150-159.

656 [39] Y. González-Espinosa, B. Sabagh, E. Moldenhauer, P. Clarke, F.M. Goycoolea,
657 Characterisation of chitosan molecular weight distribution by multi-detection asymmetric
658 flow-field flow fractionation (AF4) and SEC, Int. J. Biol. Macromol. 136 (2019) 911-919.

659 [40] D.A. Ladner, M. Steele, A. Weir, K. Hristovski, P. Westerhoff, Functionalized
660 nanoparticle interactions with polymeric membranes, J. Hazard. Mater. 211-212 (2012) 288-
661 295.

662 [41] V.R. Patel, Y.K. Agrawal, Nanosuspension: An approach to enhance solubility of drugs, J.
663 Adv. Pharm. Technol. Res. 2 (2011) 81-87.

664 [42] S. Bhattacharjee, DLS and zeta potential–What they are and what they are not? J.
665 Controlled Release 235 (2016) 337-351.

666 [43] H. Kouchakzadeh, S.A. Shojaosadati, A. Maghsoudi, E.V. Farahani, Optimization of
667 PEGylation conditions for BSA nanoparticles using response surface methodology, Aaps
668 Pharmscitech 11 (2010) 1206-1211.

669 [44] J.C. Giddings, F.J. Yang, M.N. Myers, Theoretical and experimental characterization of
670 flow field-flow fractionation, Anal. Chem. 48 (1976) 1126-1132.

671 [45] M. Baalousha, F.V.D. Kammer, M. Motelica-Heino, H.S. Hilal, P. Le Coustumer, Size
672 fractionation and characterization of natural colloids by flow-field flow fractionation
673 coupled to multi-angle laser light scattering, Journal of Chromatography A 1104 (2006) 272-
674 281.

675 [46] E. Alasonati, M. Benincasa, V.I. Slaveykova, Asymmetrical flow field-flow fractionation
676 coupled to multiangle laser light scattering detector: Optimization of crossflow rate, carrier
677 characteristics, and injected mass in alginate separation, Journal of separation science 30
678 (2007) 2332-2340.

679 [47] M. Leeman, K. Wahlund, B. Wittgren, Programmed cross flow asymmetrical flow field-
680 flow fractionation for the size separation of pullulans and hydroxypropyl cellulose, Journal
681 of Chromatography A 1134 (2006) 236-245.

682 [48] M. Andersson, B. Wittgren, K. Wahlund, Accuracy in multiangle light scattering
683 measurements for molar mass and radius estimations. Model calculations and experiments,
684 Anal. Chem. 75 (2003) 4279-4291.

685 [49] C. Ma, J. Yan, Y. Huang, C. Wang, G. Yang, The optical duality of tellurium nanoparticles
686 for broadband solar energy harvesting and efficient photothermal conversion, Science
687 advances 4 (2018) eaas9894.

688 [50] K.C. Nwoko, A. Raab, L. Cheyne, D. Dawson, E. Krupp, J. Feldmann, Matrix-dependent
689 size modifications of iron oxide nanoparticles (Ferumoxytol) spiked into rat blood cells and
690 plasma: Characterisation with TEM, AF4-UV-MALS-ICP-MS/MS and spICP-MS, Journal of
691 Chromatography B 1124 (2019) 356-365.

692 [51] J. Jiménez-Lamana, I. Abad-Álvaro, K. Bierla, F. Laborda, J. Szpunar, R. Lobinski,
693 Detection and characterization of biogenic selenium nanoparticles in selenium-rich yeast by
694 single particle ICPMS, J. Anal. At. Spectrom. 33 (2018) 452-460.

695 [52] G. Cornelis, M. Hassellöv, A signal deconvolution method to discriminate smaller
696 nanoparticles in single particle ICP-MS, J. Anal. At. Spectrom. 29 (2014) 134-144.

697 [53] B. Gómez-Gómez, J. Sanz-Landaluce, M.T. Pérez-Corona, Y. Madrid, Fate and effect of
698 in-house synthesized tellurium-based nanoparticles on bacterial biofilm biomass and
699 architecture. Challenges for nanoparticles characterization in living systems, Science of The
700 Total Environment 719 (2020) 137501.

701 [54] S. Tsuneda, H. Aikawa, H. Hayashi, A. Yuasa, A. Hirata, Extracellular polymeric
702 substances responsible for bacterial adhesion onto solid surface, FEMS Microbiol. Lett. 223
703 (2003) 287-292.

704 [55] G.H. Woehrle, J.E. Hutchison, S. Özkar, R.G. FINKE, Analysis of nanoparticle transmission
705 electron microscopy data using a public-domain image-processing program, image, Turkish
706 Journal of Chemistry 30 (2006) 1-13.

707 [56] R. Pecora, Dynamic light scattering measurement of nanometer particles in liquids,
708 Journal of nanoparticle research 2 (2000) 123-131.

709 [57] R. Peters, Y. Georgalis, W. Saenger, Accessing lysozyme nucleation with a novel dynamic
710 light scattering detector, Acta Crystallographica Section D: Biological Crystallography 54
711 (1998) 873-877.

712 [58] X.Z. Wang, L. Liu, R.F. Li, R.J. Tweedie, K. Primrose, J. Corbett, F.K. McNeil-Watson,
713 Online characterisation of nanoparticle suspensions using dynamic light scattering,
714 ultrasound spectroscopy and process tomography, Chemical Engineering Research and
715 Design 87 (2009) 874-884.

716 [59] M.M. Tosi, A.P. Ramos, B.S. Esposto, S.M. Jafari, in Anonymous Dynamic light scattering
717 (DLS) of nanoencapsulated food ingredients. Characterization of Nanoencapsulated Food
718 Ingredients. Elsevier, 2020, p. 191-211.

719 [60] A. Moquin, F.M. Winnik, in Anonymous The use of field-flow fractionation for the
720 analysis of drug and gene delivery systems. Field-Flow Fractionation in Biopolymer Analysis.
721 Springer, 2012, p. 187-206.

722 [61] S.R. Ravella, T.S. Quiñones, A. Retter, M. Heiermann, T. Amon, P.J. Hobbs, Extracellular
723 polysaccharide (EPS) production by a novel strain of yeast-like fungus Aureobasidium
724 pullulans, Carbohydrate Polymers 82 (2010) 728-732.

725 [62] S. Valueva, M. Vylegzhanina, V. Lavrent'ev, L. Borovikova, T. Sukhanova, Biogenic
726 nanosized systems based on selenium nanoparticles: Self-organization, structure, and
727 morphology, Russian Journal of Physical Chemistry A 87 (2013) 484-489.

728 [63] J. Liu, C. Liang, X. Zhu, Y. Lin, H. Zhang, S. Wu, Understanding the solvent molecules
729 induced spontaneous growth of uncapped tellurium nanoparticles, Scientific reports 6
730 (2016) 32631.

731 [64] D. Ruhland, K. Nwoko, M. Perez, J. Feldmann, E.M. Krupp, AF4-UV-MALS-ICP-MS/MS,
732 spICP-MS, and STEM-EDX for the Characterization of Metal-Containing Nanoparticles in Gas
733 Condensates from Petroleum Hydrocarbon Samples, Anal. Chem. 91 (2018) 1164-1170.

734 [65] B. Hetzer, A. Burcza, V. Gräf, E. Walz, R. Greiner, Online-coupling of AF4 and single
735 particle-ICP-MS as an analytical approach for the selective detection of nanosilver release
736 from model food packaging films into food simulants, Food Control 80 (2017) 113-124.

737 [66] B. Bocca, B. Battistini, F. Petrucci, Silver and gold nanoparticles characterization by SP-
738 ICP-MS and AF4-FFF-MALS-UV-ICP-MS in human samples used for biomonitoring, Talanta
739 220 (2020) 121404.

Characterisation of selenium and tellurium nanoparticles produced by *Aureobasidium pullulans* using a multi-method approach.

Kenneth C Nwoko[a], Xinjin Liang[b], Magali AMJ Perez[a], Eva Krupp[a], Geoffrey Michael Gadd[b,d], Jörg Feldmann[a,c]

[a.] Trace Element Speciation Laboratories, Dept. of Chemistry, University of Aberdeen, AB24 3UE, United Kingdom

[b.] Geomicrobiology Group, School of Life Sciences, University of Dundee, Dundee, DD1 5EH, United Kingdom

[c.] Institute of Chemistry, Environmental Analytical Chemistry, University of Graz, 8010 Graz, Austria

[d.] State Key Laboratory of Heavy Oil Processing, State Key Laboratory of Petroleum Pollution Control, College of Science and Environment, China University of Petroleum, Beijing, 102249, China

Abstract: *Aureobasidium pullulans* was grown in liquid culture media amended with selenite and tellurite and selenium (Se) and tellurium (Te) nanoparticles (NPs) were recovered after 30 d incubation. A separation method was applied to recover and characterise Se and Te NPs by asymmetric flow field flow fractionation (AF4) with online coupling to multi-angle light scattering (MALS), ultraviolet visible spectroscopy (UV-Vis), and inductively coupled plasma mass spectrometry (ICP-MS) detectors. Additional characterisation data was obtained from transmission electron microscopy (TEM), and dynamic light scattering (DLS). Solutions of 0.2% Novachem surfactant and 10 mM phosphate buffer were compared as mobile phases to investigate optimal AF4 separation and particle recovery using Se-NP as a model sample. 88 % recovery was reported for 0.2 % Novachem solution, compared with 50 % recovery for phosphate buffer. Different Crossflow (C_{flow}) rates were compared to further investigate optimum separation, with recoveries of 88% and 30% for Se-NPs, and 90% and 29% for Te-NPs for 3.5 mL min^{-1} and 2.5 mL min^{-1} respectively. Zeta-potential (ZP) data suggested higher stability for NP elution in Novachem solution, with increased stability attributed to minimised NP-membrane interaction due to PEGylation. Detection with MALS showed monodisperse Se-NPs (45-90 nm) and polydisperse Te-NPs (5-65 nm).Single particle ICP-MS showed mean particle diameters of 49.7±2.7 nm, and 135 ± 4.3 nm, and limit of size detection (LOSD) of 20 nm and 45 nm for Se-NPs and Te-NPs respectively. TEM images of Se-NPs and Te-NPs displayed a

spherical morphology, with the Te-NPs showing a clustered arrangement, which suggested electrostatic attraction among neighbouring particles. Particle hydrodynamic diameters (d_H) measured with dynamic light scattering (DLS) further suggested monodisperse Se-NPs and polydisperse Te-NPs distributions, showing good agreement with AF4-MALS for Se-NPs, but suggests that the R_g obtained from AF4-MALS for Te-NP was unreliable. The results demonstrate a complementary application of asymmetric flow field-flow fractionation (AF4), ICP-MS, light scattering, UV-Vis detection, and microscopic techniques to characterise biogenic Se and Te NPs.

Keywords: Biogenic nanoparticles, selenium, tellurium, AF4, ICP-MS/MS, spICP-MS

1. Introduction

Selenium (Se) and tellurium (Te) are metalloid elements that belong to the chalcogen group in Group 16 of the Periodic table. Neither selenium or tellurium are extracted as primary ores; but are recovered as by-products during the processing of base metal ores such as Cu, Pb, Bi, Fe and other metals [1]. They have an extremely low crustal abundance (Se 0.05 – 0.09 mg kg^{-1}, Te 0.02 mg kg^{-1}) and have been classified among the 'critical' elements due to a potential risk in their security of supply [2-4] . Both selenium and tellurium are of economic interest because of their applications in advanced technologies such as photovoltaic cells for solar energy, and thin film technologies[5-7] . To improve their supply, new methods of extraction have been investigated including chemical reduction[8, 9], electrochemical processes[10, 11], and microbial biorecovery[12-14] . Microbial biorecovery of Se and Te in their elemental forms may offer an environmentally sustainable, relatively low-cost method for their production at but can be challenged by the low yield and tedious purification steps to obtain sufficient amounts.[15-18]. Various species of bacteria and fungi have been investigated for the intracellular and extracellular biosynthesis of Se and Te NPs, as a means to biotransform oxyanions of both elements to less toxic forms; and their exploitation in environmental, industrial and medical applications [15-18]. Se and Te NPs biosynthesised by fungi and bacteria have shown average diameters of 60-80 nm and 221 nm respectively , and may be associated with lipid, carbohydrate and/or protein on the surface of the produced Se and Te NPs [18, 19]. Prior to any potential industrial application, there is a need to characterise biosynthesised NPs to determine their size, composition, distribution, and dispersibility. Various established kinds of metrological techniques are already in use for NP characterisation based on their

quantification, separation and characterisation with each technique providing a specific kind of information[20]. In this study, separation of the NPs was achieved with asymmetric flow field-flow fractionation (AF4), an analytical technique which sequentially separates NPs in a thin channel in order of increasing particle size under the influence of a perpendicular crossflow[21-24] . One advantage of the AF4 technique is its versatility to be simultaneously coupled with multiple detectors, with multi-angle light scattering (MALS) and inductively coupled plasma mass spectrometry (ICP-MS) detectors providing particle size data and element-specific detection, respectively and able to detect nano- and microparticles in the same run. For single particle inductively coupled plasma mass spectrometry (spICP-MS), sufficiently diluted suspensions are detected above a background signal and counted in fast time resolved analysis (TRA) mode using ultrafast integration times[25, 26] . The introduction of a single NP into the plasma generates a packet of ions creating a pulse signal when it reaches the detector. The detector pulse is correlated to the total mass per particle and subsequently correlated to the particle size[27-30] .

The main advantages of spICP-MS are that it employs the power of an ICP plasma to completely destroy any biological matrix material; it uses very small sample volumes with sufficient dilution to ensure high sensitivity of signals above background and avoid detection of two particles in one measurement event. In this study, we demonstrated the need for complementary analytical techniques to characterise biogenic nanoparticles. In addition to the coupled AF4-UV-MALS-ICP-MS and spICP-MS analytical tools, the conventional and relatively straightforward techniques such as transmission electron microscopy (TEM) and dynamic light scattering (DLS) were employed to provide an enhanced analytical perspective for a better characterisation of biogenic Se/Te-NPs produced by the polymorphic fungus *Aureobasidium pullulans* when exposed to selenite and tellurite. Many fungi are capable of the reductive transformation of metalloid oxyanions, including Se and Te, to elemental forms which provides a biological system applicable to bioremediation and/or element biorecovery[13, 31].

2. Materials and Methods

2.1 Experimental

2.1.1 Biosynthesis of NPs by *A. pullulans*. Se and Te NPs biosynthesis by A. pullulans was performed following the protocol described by Liang *et al* [18] All reagents and chemicals used

were of analytical grade or better with all volumes measured gravimetrically. Liquid cultures were prepared in 250-mL Erlenmeyer conical flasks containing 100 mL nutrient medium on an orbital shaking incubator (Infors Multitron Standard, Rittergasse, Switzerland) at 125 rpm, 25°C in the dark. AP1 agar medium was used as the growth medium with previously stated nutrient consisting of (L^{-1} Milli-Q water): D-glucose 30 g, $(NH_4)_2SO_4$ 5 g, KH_2PO_4 0.5 g, $MgSO_4 \cdot 7H_2O$ 0.2 g, $CaCl_2 \cdot 6H_2O$ 0.05 g, NaCl 0.1 g, $FeCl_3 \cdot 6H_2O$ 0.0025 g, and trace metals: $ZnSO_4 \cdot 7H_2O$ 0.004 g, $MnSO_4 \cdot 4H_2O$ 0.004 g, $CuSO_4 \cdot 5H_2O$ 0.0004 g. All chemicals, apart from D-glucose, were prepared as 1 M stock solutions and autoclaved separately (121 °C, 15 min) before appropriately combining the required volumes to reach the desired final concentrations for AP1 liquid medium. Sodium selenite (Na_2SeO_3) or sodium tellurite (Na_2TeO_3) were dissolved separately in Milli-Q water and sterilized by membrane filtration with 0.2 µm cellulose nitrate filter paper (Whatman, Maidstone, Kent, UK) and added to autoclaved AP1 medium (121^{o}C, 15 min) at room temperature to give a final concentration of 1 mM. After autoclaving, the pH of liquid medium was adjusted to pH 5 using sterile 1 M HCl. *A. pullulans* was grown on AP1 agar medium for 4 d at 25°C prior to liquid subculture. For inoculation, ten 6 mm diameter inoculum plugs were taken from the margins of actively growing colonies using sterile cork borers (autoclaved at 121°C, 15 min) and added to 100 ml AP1 medium for incubation as described above. The ability of *A. pullulans* to reduce selenite and tellurite was assessed visually, the red (Se) or black (Te) colouration being used as an indicator of reduction to their elemental forms. The culture media was filtered through cellulose nitrate membrane filters (0.45 µm pore diameter, Whatman, Maidstone, Kent, UK) to obtain suspensions free of micro-sized particles. Particles present in the fungal supernatant were harvested by centrifugation at a series of speeds (4k, 8k and 13k x g), each centrifugation step lasting 30 min until the particles in the supernatant were separated from the biomass. Harvested particles were rinsed through a graded ethanol series (50-100%(v/vaq), 15 min per step), then rinsed three times with a 20 % (w/v) sodium dodecyl sulphate (SDS) solution and finally rinsed three times with autoclaved Milli-Q water (120 °C, 15 min) to remove remaining impurities.

2.1.2 Determination of total elemental Se/Te: 50 mg of the recovered suspensions was weighed into 50 mL sample vials, 4 mL aqua regia added, pre-digested overnight in a fume hood and subsequently digested in a microwave (Mars5, CEM Microwave Technology Ltd,

Buckingham, UK) using the open vessel method[32] . Trace element calibration standards (VWR, USA) in the range 1 µg L^{-1} to 100 µg L^{-1} were prepared and analysed for quantification of Se/Te by external calibration with inline addition of 10 µg L^{-1} Ge was used as an internal standard to monitor plasma fluctuation and cancel out sensitivity shifts. All analysis was performed in triplicate and errors reported as standard deviation.

2.1.3 Preparation of AF4 carrier solutions. AF4 carrier solutions were prepared fresh daily before measurement with de-ionised water (18.2 Ω cm) obtained from a Millipore system. Novachem surfactant (Postnova Analytics Landsberg, Germany) was diluted with de-ionised water in a 1000 mL volumetric flask to reach a concentration of 0.2% v/v. The Novachem surfactant is a mixture of cationic and anionic surfactants as follows (in wt.%): water 88.8, triethanolamine oleate 3.8, sodium carbonate 2.7, alcohols + C12-14-secondary ethoxylate 1.8, tetrasodium ethylenediaminetetraacetate 1.4, polyethylene glycol 0.9, sodium oleate 0.5, sodium bicarbonate 0.1. 10 mM phosphate buffer was prepared by dissolving 8 g of NaCl, 200 mg KCl, 240 mg KH_2PO_4, and 1.44 g Na_2HPO_4, in 800 mL of deionised water. The pH was adjusted to 7.4 with aqueous ammonia and deionised water added to a final volume of 1000 mL. Both solutions were stirred for 10 min and vacuum filtered through a 0.45 µm cellulose acetate filter.

2.1.4 Sample preparation for spICP-MS. 0.5 mL samples were transferred to 1.5 mL Eppendorf vials fitted with 10 kDa cut-off mesh. Vials were centrifuged at 10,000 x *g* for 3 min, the supernatant was discharged, and the pellets rinsed with 0.5 mL deionised water. The process was repeated, and the final pellet was resuspended in 0.5 mL deionised water, then transferred to 15 mL plastic tubes. Filtered samples were diluted with deionised ultrapure water prior to spICP-MS analysis. Transport efficiency was determined with measurement of a 50 mg kg^{-1} AuNP colloidal suspension (Nanocomposix, USA) with a nominal diameter of 60 nm as a reference standard since Se or Te nanoparticle certified reference standards are not currently available. The Au-NP suspension was diluted by a factor of 10^{-6} to give a final concentration of 50 ng kg^{-1}. Elemental aqueous standards of Se and Te of 1 µg L^{-1} were prepared for the determination of elemental response factors. All samples were bath sonicated at 37 kHz for 10 min before analysis.

2.2 Instrumental analysis

2.2.1 AF4-UV-MALS. AF4 analysis was performed with a metal-free AF 2000 system (Postnova Analytics, Landsberg, Germany), with inbuilt software for data acquisition. The separation system consisted of a solvent degasser, solvent organiser, two isocratic solvent pumps, a pair of Kloehn pumps for generation of the crossflow, an auto-sampler, and a separation channel. The separation channel consisted of a trapezoid cartridge, fitted with a spacer of 350 μm nominal height and a regenerated cellulose acetate membrane with molecular weight cut-off (MWCO) of 10 kDa as the accumulation wall. The auto-sampler and oven temperatures were maintained at 4 ^{o}C and 20 °C, respectively. The AF4 system was coupled to UV-Vis, multi-angle light scattering (MALS) detectors and an ICP-MS through an interface system. The MALS detector consisted of 21 light scattering cells at angles between 7^{o} and 164^{o}, with a laser light intensity of 50 mW and wavelength of 532 nm. A sample volume of 20 μL was maintained throughout, with at least triplicate injections per sample. Sample carryover was eliminated by injecting 1 % HNO_3 solution for 5 min after each run to flush the AF4 channel.

2.2.2 ICP-MS/MS: ICP-MS/MS analysis was performed using an Agilent 8800 ICP-MS/MS (Agilent Technologies, Santa Clara, USA) instrument. The ICP-MS instrument was fitted with a Micromist nebulizer and a Scott double pass spray chamber. ICP-MS/MS operating conditions are listed in Table S1.

2.2.3 spICP-MS: Single particle ICP-MS analysis was performed using an Agilent 7900 ICP-MS equipped with a Micromist nebulizer, double pass spray chamber and an autosampler. The system was fitted with a quartz torch with internal diameter of 1 mm to reduce signal background and improve sensitivity. Nanoparticle diameters for all the samples were reported as an average diameter of six replicates. Collision cells were pressurised with 3.5 mL min^{-1} H_2 gas in both ICP-MS/MS and sp-ICP-MS measurements to remove interfering species. Instrumental parameters (lens position, torch position) were optimised daily to achieve maximum sensitivity with an aqueous tune solution of 10 µg L^{-1} Li, Co, Y, Ce, Tl. Data analysis was performed using Agilent MassHunter 4.4 software (Agilent Technologies, USA).

2.2.4 TEM: Samples were bath sonicated at 37 kHz for 5 min and 5 μL aliquots transferred using a micropipette onto a Formvar-coated 200-mesh copper grid and left to dry in ambient conditions for 20 min. TEM Images were acquired with a JEOL-1400 plus electron microscope, at an accelerating voltage of 80 kV, using an AMT UltraVUE camera. After image acquisition,

they were filtered, and individual points were counted as NPs using ImageJ processing software, assuming a spherical morphology for the NPs; particle diameters were calculated from areas of individual spheres.

2.2.5 Dynamic light scattering (DLS): DLS analysis in batch mode was performed with a Malvern Zetasizer Nano ZS (Malvern Panalytical, Worcestershire, UK) system with a He-Ne laser as the light source at 632 nm and 173° scattering angle. Samples were dispersed in deionised water with refractive index (1.33), viscosity (8.9×10^{-4} Pa s) and temperature (25°C) inputted into the measurement file. The sample suspensions were diluted 1:100 *v/v* with deionised water followed by 120 s equilibration time. Average particle sizes based on scattered light intensity weighted averages were automatically calculated by the software based on the Stokes-Einstein theory and reported as hydrodynamic diameters. The instrument also enabled the determination of the zeta-potential under same instrumental settings with equilibration time of 120 s. The determination of the zeta-potential was based on the Smoluchowski model with a Henry's Function F(Ka) of 1.5.

3. Results and Discussion

3.1 Total biogenic SeNPs and TeNPs generated by *A. pullulans*

After 30-day incubation, nanoparticles were harvested from supernatants of *A. pullulans* after growth in AP1 medium amended with 1 mM Na_2SeO_3 (79 mg Se L^{-1})/Na_2TeO_3 (128 mg Te L^{-1}). Total yields of SeNPs and TeNPs harvested from the supernatant were 81.6 ± 1.4 mg L^{-1}, 21.5 ± 0.1 mg L^{-1} (*n=3*) respectively. Previous research has already demonstrated that SeNPs and TeNPs can be located both intracellularly and extracellularly[18, 33]this work focused on the extracellular SeNPs and TeNPs harvested from the fungal supernatant because of their relative ease of separation from the biomass and media. It appeared that the biotransformation of selenite to elemental selenium was quantitative while the biotransformation from tellurite to elemental tellurium saw only resulted in a conversion of 16.8%. Se and Te species can betoxic to microbes, with Te reported to show higher toxicity at lower concentrations than Se [34]. In some microbes, Te-oxyanions such as tellurite react with thiols such as glutathione (GSH); which supports the conversion of tellurite to elemental tellurium [35]. The low yield of Te-NPs by *A.pullulans* is therefore suggested to be linked to Te toxicity which though is not fully understood in fungi, could be caused by the accumulation

of reactive oxygen species (ROS) as a result of depletion of GSH and resultant loss of anti-oxidant capability.

3.2 **AF4 method development and optimisation**

From field-flow fractionation (FFF) theory, retention time (t_r) is directly proportional to particle size and is dependent on parameters such as absolute temperature, area of the accumulation wall, crossflow rate, viscosity of the mobile phase, channel flow, and channel thickness[21, 22] . A combination of AF4 parameters such as membrane type, crossflow rate (C_{flow}), focus flow rate, channel thickness, ionic strength of carrier, and sample load have been established to influence optimum separation and recovery in the AF4 technique to various degrees[36, 37] . In our study, AF4 separation parameters of mobile carrier and C_{flow} rates were investigated for their influence on recovery and elution of the Se/Te-NPs. The 0.2% v/v Novachem solution was compared with a buffer solution, (10 mM phosphate buffer, pH=7.4), to compare their suitability as an AF4 mobile carrier for the microbial sample matrices. Recoveries obtained from UV-Vis signals (Figure 1) were compared with the peak area of an injection without a C_{flow}, using the formula (Equ. 1) [38] :

$$R\ (\%) = A/A_0 \times 100 \qquad \text{Equ. 1}$$

where, A= Peak area obtained with a crossflow
A_0= Peak area without an applied crossflow

Recoveries of 88% and 50% were recorded for the Se-NPs using 0.2% v/v Novachem solution and 10 mM phosphate buffer, respectively. Both 0.2% v/v Novachem solution and 10 mM phosphate buffer influenced the analyte retention times; the Se-NP peak was observed at 26 min in 0.2% v/v Novachem solution, and 30 min in phosphate buffer. This indicated that the surface of SeNPs were modified with phosphate buffer which could be due to an electrostatic effect, such that the SeNPs have lower surface charges resulting in a higher level of membrane adsorption and consequently elute later. The electrostatic effect might also be related to the ζ-potential (ZP) of the NPs (Table 1). A net negative surface ZP has been reported for the 10 kDa membrane in past studies [39, 40]. Theoretically, lower ZP values might indicate lower stability and promote aggregation/adhesion, while higher ZP values would indicate better stability [41]. The phosphate ions would be expected to impart a negative charge to the Se-NPs which would enhance repulsion between the membrane and surface NPs, but this

appears not to be the case, as attractive forces appear to be present. Also, the higher ionic strength may also increase the compression of the electric double layer (EDL) and decrease ZP [42]. Furthermore, it appears that polyethylene glycol (PEG) in the Novachem surfactant facilitates the formation of a PEGylated corona around the NP which increases its stability [43]and may minimize interaction with the membrane which consequently improves recovery. Though maximum electrostatic repulsion determined by ZP measurements is required to ensure minimal contact between the NPs surface and the membrane, it is challenging to explain electrostatic attractive forces which may be present (such as Van der Waals forces). Therefore, ZP data must be interpreted and applied with caution. Also, accurate ZP measurements in cell culture medium are challenging because of their enrichment with ions which increases conductivity and interferes with ZP measurement [42].

Table 1 ZP values of Se-NP and Te-NP dispersed in AF4 running solutions

Figure 1. Representative AF4-MALS-UV fractograms depicting the effect of mobile phases using 0.2% v/v Novachem solution (NVC, red traces) in comparison with 10mM phosphate buffer (PO_4; black traces); as detected by light scattering (LS 90°) (top fractogram)and UV-Vis (bottom fractogram) at 280 nm wavelength. Novachem solution demonstrated faster elution and better analyte recovery (88%) than phosphate buffer (50%). Analysis conditions for AF4 are reported in Table S2 (Supplementary information).

To optimise the AF4 method, an elution programme with an optimal C_{flow} rate was investigated and sample recoveries monitored with the UV-Vis, MALS and ICP-MS/MS detectors with recovery calculations shown with ICP-MS/MS signals (Figure 2). A 2 mL min^{-1} C_{flow} resulted to a narrow Se peak at 17 min (30% recovery), compared to the 88% recovery rate with a C_{flow} of 3.5 mL min^{-1}, with a symmetrical monodisperse peak. Similarly, TeNPs eluted with C_{flow} 3.5 mL min^{-1} also showed a larger peak area with higher recovery (90%) compared to Te-NPs eluted at 2 mL min^{-1} with low recovery (29%). Separation with a 3.5 mL min-^{1} crossflow, showed larger peak areas and consequently better analyte recoveries with clearer separation of peaks. C_{flow} rate is a critical AF4 separation parameter [44, 45]. Though it is expected from FFF theory that a higher crossflow increases the chances of membrane

adhesion and poor recovery [46], previous studies have reported that the filtration of complex samples prior to injection improves analyte recovery [39]. It appears that filtration through a 0.45 µm cellulose acetate filter significantly reduced the amount of biological debris and micro-sized particles in the sample matrix which would otherwise adhere to the membrane. Another possible explanation for this observation is that the higher repulsion generated between the negatively charged Se-NP and the negative ZP of the membrane causes the particle to diffuse faster, hence shorter time and also higher recovery.

Figure 2. AF4-ICP-MS/MS fractograms depicting the comparison of different C_{flow} rates on the recovery of Se-NP (red traces) and Te-NP (black traces using 0.2% v/v Novachem solution as mobile phase. C_{flow} rates of 3.5 mL min^{-1} (bottom fractogram, B) for both Se-NP and Te-NP indicated higher analyte recovery compared with C_{flow} of 2.0 mL min^{-1}. Analytical conditions for ICP-MS/MS are reported in Table S1 (Supplementary information).

The C_{flow} programme in exponential decay mode applied in this study consumed more carrier liquid compared to a linear-mode, but it provided a better separation resolution, recovery, and sensitivity for aggregated samples. It also has been validated in the AF4 separation of pullulan and hydroxypropyl cellulose by Leeman *et al* [47] . Moreover, the Se-NP peak appeared towards the end of the applied C_{flow} in the elution programme, suggesting that the Se-NPs have a reversible, strong attractive force towards the membrane in contrast to the Te-NPs which completely eluted within the elution timeframe with an applied C_{flow}.

3.3 **Particle sizing by AF4-MALS**

Radii of gyration were computed from MALS signals based on a spherical fit model and showed good data fit across the light scattering angles (Figure S1). The MALS detector was calibrated using 5 mg/mL bovine serum albumin (BSA) and 0.2% Novachem solution as eluent as recommended by the instrument manufacturer's protocol (Postnova Analytics GmbH). A molar weight of 66,000 g/mol was recorded for BSA with the application of 0.185 mL/g for

refractive index increment (dn/dc) while the second virial coefficient was considered negligible considering the very dilute concentrations typical of AF4 separations [48].

Se-NPs showed a particle size range of 45 nm – 90 nm with a mean R_g value of 80.0 nm and appeared monodisperse; while Te-NPs showed a mean R_g of 29.5 nm, within a range of 5 nm to 65 nm and were polydisperse. The Te-NP ICP-MS/MS traces (Figure 2) clearly highlighted the detection of three fractions of Te-NPs between 4 min (t_0) and 15 min, which are not visible from the MALS trace (Figure. 3B), demonstrating the higher sensitivity and specificity of ICP-MS/MS over MALS detection. Furthermore, intense UV-Vis signals for both elements suggested the detection of light absorbing biomolecules in the NPs, which have been previously reported to be extracellular polymeric substances (EPS) secreted by *A. pulluans*[18] The UV-Vis- and MALS peaks for Se-NPs (Figure S3) appeared to be well-overlaid suggesting that the EPS surrounded the Se-NPs surface. However, the UV-Vis peak however shows a peak at around 20 min without a corresponding MALS signal, which suggests a different biomolecule present in the EPS which is not bound to the NP. For the Te-NPs, the UV-Vis signal showed two peaks between 20 min and 25 min which also suggested the presence of multiple biomolecules present in the EPS. The MALS signal was detected at 30 min,suggesting the detection of large sized non-Te containing NP, while the fraction of EPS detected with UV-Vis (20-25 min) showed the absence of light scattering molecules. It can be inferred that the Te-NPs were unstable and disintegrate in the channel during separation. Also, Te-NPs below 100 nm have been reported to exhibit plasmonic-like scattering like Au-NPs[49]and in this case appeared to interfere with the light scattering signal which may explain the near absent MALS signal between 4 and 15 min.

Figure 3. AF4-MALS fractograms of Se-NPs (top fractogram, A) and Te-NPs (bottom fractogram, B) detected by light scattering ((LS 90°) on the left axis, and radius of gyration (R_g) on the right axis, with size computation based on a spherical fit model. Demonstration of data fit across light scattering angles is depicted in Figure S1 (Supplementary information). Se-NPs showed a narrow monodisperse structure with a range of 45-90 nm, while Te-NPs were polydisperse with a 5-65 nm.

3.4 Single particle ICP-MS

In single particle ICP-MS (spICP-MS), particle diameter is dependent on the total mass introduced into the plasma through the nebulizer (transport efficiency), which in this study

was calibrated against a 50 ng kg^{-1} Au-NP (60 ± 5 nm) certified reference material following the protocol reported in our previous work[50] . The spICP-MS results showed a median particle diameter 49.7±2.7 nm for Se-NPs, and a limit of size detection (LOSD) of 20 nm, attributed to reduced background signal levels. This reduced background signal arose from a number of factors: measurement of the more abundant ^{78}Se isotope and removal of argon dimer (^{40}Ar ^{38}Ar) interference resulting from the addition of H_2 gas to the collision cell[51]; and the ultracentrifugation of the samples with a 10 kDa cut-off filter during sample preparation which removed excess dissolved Se/Te from the samples and consequently reduced the background.

Figure 4. Time scans and particle size-frequency distribution of NP signals acquired for Se(A), and Te(B) at a dwell time of 0.1 ms. MassHunter software analysis indicated a median diameter of 49.7±2.7 nm Se-NPs, and 135±0.3 nm Te-NPs. Limits of size detection (LOSD) were 20 nm, and 45 nm for Se-NP and Te-NP, respectively. Analytical conditions for sp-ICP-MS are reported in Table S1 (Supplementary information).

The Te-NPs showed a median diameter of 135 ± 0.3 nm and are therefore significantly larger than the SeNPs. However, the particle-size distribution (PSD) is not normally distributed because the measurement of a NP suspension with spICP-MS always produces a combined signal containing both dissolved ions and particles. Thus, in calculating the PSD frequencies of a NP suspension, the instrumental software assumes that the lowest intensities in the histogram arose from particle free measurements. However, the dissolved analyte signal actually contributes to the determination of the PSD, despite of the apparent removal of dissolved analyte signal from the data during PSD calculations[52] . This is responsible for the LOSD of 45 nm for Te-NPs, which was an improvement from the LOSD of 80 nm for biogenic Te-NPs reported by Gómez-Gómez *et al.* [53]. Like in the case of the Se-NP, this also appeared to be related to the removal of excess dissolved tellurium using the ultracentrifugation cut-off membrane and subsequent dilution of the samples. However, one disadvantage of the ultracentrifugation step could be the loss of smaller sized NPs, which may cause a bias in particle counting in favour of larger sized particles as seen with the Te-NPs. In addition, enhanced particle detection and counting was achieved in this study with a 0.1 ms dwell time compared with a 3 ms dwell time reported in the study by Gómez-Gómez [53] . Mean R_g (80 nm) from AF4-MALS correlated with the median diameters (49.7 nm) recorded by spICP-

MS for Se-NPs (which represents only Se, assuming a core of only Se). AF4-MALS R_g values suggested a corona surrounding the Se-NP, which was likely to be secreted extracellular protein from the fungi which behave as capping agents[54] .

3.5 **TEM**

Microscopic examination is a conventional, fast, direct, and simple technique to examine NP morphology and determine core particle diameters (as equivalent circular diameters) by counting the number of representative particles as originally reported by Woehrle *et al*[55] . TEM images indicated spherical morphologies for both NPs, but the Te-NPs were arranged in clusters or aggregates while the Se-NPs were randomly distributed (Figure. 5).

Figure 5. TEM images (top left and bottom left) and frequency size graphical distributions (top right and bottom right) of Se-NPs (A) and Te-NPs (B). Se-NPs displayed spherical shapes and randomly distributed, while Te-NPs displayed a clustered arrangement.

The formation of clusters can be attributed to electrostatic interactions from functional groups present in the proteins and polysaccharides contained in the extracellular polymeric substances (EPS) which have been associated with biogenic tellurium recovered from fungal biomass [14] . The TEM average particle diameters for Se-NP (35.5±2.5 nm) were comparable with spICP-MS (49.7±2.7 nm) and reflected a more realistic particle size since the NPs measured with TEM did not undergo additional sample preparatory steps such as dilution and centrifugation which might alter particle size. TEM also captures smaller sized particles below the particle LOSD recorded with spICP-MS (10 nm for Se-NP, 15 nm for Te-NP) which makes it an attractive technique for measurement of ultrasmall NPs. However, TEM measures only a small proportion of the sample and therefore assesses fewer number of particles compared to AF4 and spICP-MS.

3.6 **Particle sizing by dynamic light scattering (DLS)**

DLS provides a quick non-invasive, non-specific technique to obtain particle size distributions (as hydrodynamic diameters, d_H) and polydispersity index of colloids in solution. DLS theory is based on correlating the light scattered by particles and undergoing Brownian motion, to their size and shape based on the Stokes-Einstein equation[56]. Irradiation of colloidal

particles dispersed in a liquid medium by a laser source causes changes in light intensity over time; these changes are related to the particle diffusion coefficient. Bigger particles diffuse slowly causing changes in the intensity of scattered light over a larger time scale, while the smaller particles move faster. Therefore, an ideal solution for DLS must be sufficiently diluted and free of large particles that can cause interference. To minimise multiple scattering and interference from artefacts such as dust, the DLS instrument was equipped with non-invasive backscattering (NIBS) which detects scattered light at a 173° angle[57, 58] . Quality control of DLS data was ensured by measuring latex particles (diluted in water), showing diameters of 64 ± 2.6 nm and 131 ± 2.5 nm which were within range of certified values (60 ± 3 nm, and 125± 2 nm) respectively. Samples were measured at least in triplicates at least and showed good reproducibility of peaks for Se-NPs, while in Te-NPs, the overlaid peaks suggested non-uniform scattering that may be caused by the presence of aggregates. A polydispersity index (PDI) below 0.7 suggests a monodisperse NP distribution while values above 0.7 are considered polydisperse[59] . Se-NPs showed a monodisperse distribution (Figure 6) with a polydispersity index of 0.2, while Te-NPs showed a polydispersity index of 0.7 and were therefore considered more polydisperse. Since both AF4-MALS and DLS provide the particle size as an ensemble, both techniques can therefore be directly compared. This can also be attributed to calculation methodologies used for both DLS and MALS which work well for monodisperse samples but are not always appropriate for polydisperse samples[60] ..

Figure 6. DLS fractograms showing intensity weighted distributions for Se-NPs (A) and Te-NPs (B) at the top half of the panel and overlay of triplicate analysis of Se-NPs (C) and Te-NPs (D). Average diameters of 167±1.4 nm and 174 ± 2.1 nm were recorded for Se-NPs and Te-NPs.

A summary of the particle radii obtained from the different techniques reflected the different principles of each technique (Table 2). Theoretically, DLS and AF4-MALS measure the size of the particle core and any surrounding material including the surface coating which may be contributed by stabilizing agents. spICP-MS measures the size distribution of the inorganic NP particle core from its elemental mass, while TEM is a non-specific technique which applies transmitted electrons which enables the visualisation and counting of the “particles” on the

sample grid, which may sometimes include particle aggregates. Therefore, particle sizes obtained from DLS cannot be accurately compared with spICP-MS because DLS is very non-specific and measures hydrodynamic diameter while spICP-MS measures the diameter of a single spherical particle and is element specific, i.e., it reports the size of the Se or Te core of the Se-NP and Te-NP, respectively. DLS must therefore be considered only as a screening approach to investigate the presence or absence of submicron particles regardless of their chemical composition.

For Se-NPs, Table 2 showed that the mathematical radius detected with spICP-MS was 1/3 of the hydrodynamic radius (R_H) detected with AF4-MALS and DLS, with the latter two techniques showing good agreement (Table 2). The AF4-MALS and DLS data can be possibly attributed to a corona surrounding the Se-NP core comprising a solvent hydration layer, adsorbed salts on the NP surface, and extracellular polymeric substances (EPS) secreted by *A. pullulans* [61, 62]; with an assumption that the particle has a pure elemental selenium core. The particle sizes of the Se-NP measured with spICP-MS and TEM are comparable considering that the spICP-MS average particle radius of 25 nm was close to its limit of size detection (LOSD) of 20 nm reported for Se-NPs. The TEM images of Se-NPs also appeared randomly distributed suggesting some overlap between smaller and larger sized particles, which makes it challenging for the ImageJ software to assign an accurate average particle size.

The Te-NPs showed a distinct difference from the Se-NPs. Particle radii from DLS were far higher than AF4-MALS and may suggest non-uniform light scattering caused by the presence of aggregates in the sample. Excessive aggregation detected by the DLS technique for Te-NPs compared to Se-NPs is evident from their standard deviation values (±3.1 vs ±0.9). The AF4-ICP-MS/MS and AF4-MALS fractograms (Figure 2B and 3B) also suggested a highly aggregated and polydisperse sample distribution with 4 Te-NPs size fractions which were more clearly detected by AF4-ICP-MS/MS (Figure 2B). AF4-MALS (Figure 3B) and AF4-UV (Figure S3) peaks were observed between 20 and 30 min but were undetected with AF4-ICP-MS/MS (Figure 2B) which strongly suggested the presence of biomolecules or EPS which have detached from the Te-NP surface.

Furthermore, the ultra-small sized TeNPs detected at the beginning of the AF4-ICP-MS/MS and AF-MALS fractograms might induce a high surface free energy that accelerated the aggregation of adjacent Te-NPs, which resulted in unreliable particle data when light scattering techniques (AF4) were applied. Moreover, the relative less dense surface coating

of the Te-NPs might cause the numerous unsaturated coordination sites on the NP surface to easily absorb or bond with the solvent molecules[63] . It is also possible that the aggregated NPs became unstable and broke down in the AF4 channel, as reported for mercury NPs by Ruhland *et al*. [64]. spICP-MS measures the aggregates as one whole particle without breaking them up resulting in an apparent larger average particle radius (67 nm) ; with the highest standard deviation (±4.3) amongst the 4 techniques further suggesting that the Te-NPs were heterogeneously distributed and more polydisperse than the Se-NPs. The TEM images showed a tightly clustered distribution which further indicated that the Te-NPs tend to form aggregates. The TEM average particle radius of 19.5 nm further supports the observation of a tightly clustered distribution which might be a result of strong electrostatic interaction between the Te-NPs and the surrounding medium.

Table 2. Summary of particle sizes measured with the different techniques. Errors are given as standard deviation of triplicates; diameters and mathematical radius are shown (in parentheses).

4. Conclusions

Selenium and tellurium nanoparticles were harvested from *A. pullulans* grown in liquid medium amended with sodium selenite and sodium tellurite for 30 days and characterised using different techniques. Based on the results presented in this work, the NPs have been separated with field-flow fractionation and characterised (particle size, shape, morphology, and distribution) with mass spectrometry and optical techniques. Various flow and sample parameters influence an optimal AF4 separation, and therefore a minimal number of parameters should be identified during an analytical study to conserve time and resources. The major advantage of AF4 fractionation is its capability to be simultaneously coupled with multiple detectors to achieve high resolution NP separation from a complex matrix, particle concentration, size distribution, elemental detection in one single run. The coupling of AF4-MALS-UV with spICP-MS analysis for inorganic nanoparticle detection has been reported [65, 66], an inability to couple both techniques was therefore considered to be a major limitation of this study. To achieve optimal separation with asymmetric flow field-flow fractionation (AF4), a surfactant-based carrier solution and a high crossflow were applied which showed particularly good recoveries and resolution. Based on their elution behaviour, Se-NPs and Te-

NPs displayed different particle physico-chemical properties and flow behaviour in the AF4 channel. ICP-MS showed high sensitivity over MALS particularly with the detection of ultrasmall Te-NPs. Particle diameters obtained from spICP-MS suggested either a bias in favour of the counting of larger sized particles, or aggregation especially for Te-NPs. Improvement in LOSD for Se and Te measured with spICP-MS demonstrated the reliability of our data and is an improvement on previous studies. Though TEM and DLS are non-specific and regarded as conventional and relatively easy techniques, they are strong tools to provide imaging and size distribution for NPs, requiring low sample volumes and providing easily interpretable data. As ensemble sizing techniques, DLS and MALS data showed good agreement for a monodisperse Se-NP with dense polymer layer which was free of aggregates, while suggesting the detection of polydisperse Te-NP aggregates. The study has contributed further to understanding the nature of biogenic Se and Te NPs and their characterization and illustrated that a multi-method approach is necessary to characterise these natural NPs in a more holistic way.

Declaration of Conflicting Interests

None

Acknowledgements

KCN acknowledges the receipt of joint PhD research funding received from the University of Aberdeen's Elphinstone studentship award, and the Federal Government of Nigeria through the Niger-Delta Development Commission (NDDC) Foreign Postgraduate Scholarship Scheme. JF and KCN gratefully acknowledge Postnova Analytics, UK for loaning of the AF4 system and technical support, and the Microscopy and Histology Facility at the Institute of Medical Sciences, University of Aberdeen for TEM measurements. G.M.G. gratefully acknowledges research support from Natural Environment Research Council (NE/M010910/1) under the NERC Security of Supply of Mineral Resources Grant Programme: Tellurium and Selenium cycling and supply (TeaSe).

Authorship contribution statement

Kenneth C Nwoko: Writing-original draft, review and editing, sample preparation, instrumental analysis (AF4-UV-MALS-ICP-MS/MS), DLS, TEM.

Xinjin Liang: Growth and culture experiments, review, editing.

Magali AMJ Perez: Sample preparation and instrumental analysis (spICP-MS, TEM).

Eva Krupp: Supervision.

Geoffrey Michael Gadd: Conceptualization, supervision, funding acquisition, review, editing.

Jörg Feldmann: Conceptualization, supervision, funding acquisition, review, editing.

References

[1] M. Bouroushian, in Anonymous Chalcogens and Metal Chalcogenides. Electrochemistry of Metal Chalcogenides. Springer, 2010, p. 1-56.

[2] Z. Hu, S. Gao, Upper crustal abundances of trace elements: a revision and update, Chem. Geol. 253 (2008) 205-221.

[3] L.T. Peiró, G.V. Méndez, R.U. Ayres, Material flow analysis of scarce metals: Sources, functions, end-uses and aspects for future supply, Environ. Sci. Technol. 47 (2013) 2939-2947.

[4] S.C. Spinks, J. Parnell, D. Bellis, J. Still, Remobilization and mineralization of selenium–tellurium in metamorphosed red beds: evidence from the Munster Basin, Ireland, Ore Geology Reviews 72 (2016) 114-127.

[5] S. Davidsson, M. Höök, Material requirements and availability for multi-terawatt deployment of photovoltaics, Energy Policy 108 (2017) 574-582.

[6] A. Naumov, Selenium and tellurium: state of the markets, the crisis, and its consequences, Metallurgist 54 (2010) 197.

[7] S. Wang, Tellurium, its resourcefulness and recovery, JOM 63 (2011) 90.

[8] F. Zhang, Y. Zheng, G. Peng, Selection of reductants for extracting selenium and tellurium from degoldized solution of copper anode slimes, Transactions of Nonferrous Metals Society of China 27 (2017) 917-924.

[9] H. Pasdar, B. Hedayati Saghavaz, M. Masoumi, A simple method for the recovery of selenium from copper anode slime sample using alkaline roasting process, International Journal of New Chemistry 6 (2019) 143-150.

[10] Y. Wang, Y. Xue, J. Su, S. Zheng, H. Lei, W. Cai, W. Jin, Efficient electrochemical recovery of dilute selenium by cyclone electrowinning, Hydrometallurgy 179 (2018) 232-237.

[11] W. Jin, J. Su, S. Chen, P. Li, M.S. Moats, G. Maduraiveeran, H. Lei, Efficient electrochemical recovery of fine tellurium powder from hydrochloric acid media via mass transfer enhancement, Separation and Purification Technology 203 (2018) 117-123.

[12] A. Ramos-Ruiz, J.A. Field, J.V. Wilkening, R. Sierra-Alvarez, Recovery of elemental tellurium nanoparticles by the reduction of tellurium oxyanions in a methanogenic microbial consortium, Environ. Sci. Technol. 50 (2016) 1492-1500.

[13] X. Liang, M.A.M. Perez, S. Zhang, W. Song, J.G. Armstrong, L.A. Bullock, J. Feldmann, J. Parnell, L. Csetenyi, G.M. Gadd, Fungal transformation of selenium and tellurium located in a volcanogenic sulfide deposit, Environ. Microbiol.(2020) .

[14] J. Mal, Y.V. Nancharaiah, N. Maheshwari, E.D. van Hullebusch, P.N.L. Lens, Continuous removal and recovery of tellurium in an upflow anaerobic granular sludge bed reactor, Journal of Hazardous Materials 327 (2017) 79-88.

[15] R. Borghese, M. Brucale, G. Fortunato, M. Lanzi, A. Mezzi, F. Valle, M. Cavallini, D. Zannoni, Reprint of “Extracellular production of tellurium nanoparticles by the photosynthetic bacterium Rhodobacter capsulatus”, J. Hazard. Mater. 324 (2017) 31-38.

[16] E. Zonaro, E. Piacenza, A. Presentato, F. Monti, R. Dell’Anna, S. Lampis, G. Vallini, Ochrobactrum sp. MPV1 from a dump of roasted pyrites can be exploited as bacterial catalyst for the biogenesis of selenium and tellurium nanoparticles, Microbial cell factories 16 (2017) 1-17.

[17] E.J. Espinosa-Ortiz, E.R. Rene, F. Guyot, E.D. van Hullebusch, P.N.L. Lens, Biomineralization of tellurium and selenium-tellurium nanoparticles by the white-rot fungus Phanerochaete chrysosporium, Int. Biodeterior. Biodegrad. 124 (2017) 258-266.

[18] X. Liang, M.A.M. Perez, K.C. Nwoko, P. Egbers, J. Feldmann, L. Csetenyi, G.M. Gadd, Fungal formation of selenium and tellurium nanoparticles, Appl. Microbiol. Biotechnol. 103 (2019) 7241-7259.

[19] E. Zonaro, S. Lampis, R.J. Turner, S.J.S. Qazi, G. Vallini, Biogenic selenium and tellurium nanoparticles synthesized by environmental microbial isolates efficaciously inhibit bacterial planktonic cultures and biofilms, Frontiers in microbiology 6 (2015) 584.

[20] N.L. Pacioni, in Anonymous Metrology for Metal Nanoparticles. Handbook of Ecomaterials. Springer, 2018, p. 1-16.

[21] M.E. Schimpf, K. Caldwell, J.C. Giddings, Field-flow fractionation handbook. John Wiley & Sons, 2000, .

[22] H. Lee, S.K.R. Williams, J.C. Giddings, Particle size analysis of dilute environmental colloids by flow field-flow fractionation using an opposed flow sample concentration technique, Anal. Chem. 70 (1998) 2495-2503.

611 [23] J.C. Giddings, Field-flow fractionation: analysis of macromolecular, colloidal, and
612 particulate materials, Science 260 (1993) 1456-1465.

613 [24] P. Li, J.C. Giddings, Isolation and measurement of colloids in human plasma by
614 membrane-selective flow field-flow fractionation: Lipoproteins and pharmaceutical colloids,
615 J. Pharm. Sci. 85 (1996) 895-898.

616 [25] C. Degueldre, P. Favarger, S. Wold, Gold colloid analysis by inductively coupled plasma-
617 mass spectrometry in a single particle mode, Anal. Chim. Acta 555 (2006) 263-268.

618 [26] C. Degueldre, P. Favarger, Colloid analysis by single particle inductively coupled plasma-
619 mass spectroscopy: a feasibility study, Colloids Surf. Physicochem. Eng. Aspects 217 (2003)
620 137-142.

621 [27] W. Lee, W. Chan, Calibration of single-particle inductively coupled plasma-mass
622 spectrometry (SP-ICP-MS), J. Anal. At. Spectrom. 30 (2015) 1245-1254.

623 [28] G. Cornelis, M. Hassellöv, A signal deconvolution method to discriminate smaller
624 nanoparticles in single particle ICP-MS, J. Anal. At. Spectrom. 29 (2014) 134-144.

625 [29] F. Laborda, J. Jiménez-Lamana, E. Bolea, J.R. Castillo, Selective identification,
626 characterization and determination of dissolved silver (I) and silver nanoparticles based on
627 single particle detection by inductively coupled plasma mass spectrometry, J. Anal. At.
628 Spectrom. 26 (2011) 1362-1371.

629 [30] W. Haiss, N.T. Thanh, J. Aveyard, D.G. Fernig, Determination of size and concentration
630 of gold nanoparticles from UV− Vis spectra, Anal. Chem. 79 (2007) 4215-4221.

631 [31] X. Liang, G.M. Gadd, Metal and metalloid biorecovery using fungi, Microbial
632 biotechnology 10 (2017) 1199-1205.

633 [32] A. Raab, M. Stiboller, Z. Gajdosechova, J. Nelson, J. Feldmann, Element content and
634 daily intake from dietary supplements (nutraceuticals) based on algae, garlic, yeast fish and
635 krill oils—Should consumers be worried? Journal of Food Composition and Analysis 53
636 (2016) 49-60.

637 [33] F.G. Martínez, G. Moreno-Martin, M. Pescuma, Y. Madrid-Albarrán, F. Mozzi,
638 Biotransformation of selenium by lactic acid bacteria: formation of seleno-nanoparticles and
639 seleno-amino acids, Frontiers in Bioengineering and Biotechnology 8 (2020) 506.

640 [34] T.G. Chasteen, D.E. Fuentes, J.C. Tantaleán, C.C. Vásquez, Tellurite: history, oxidative
641 stress, and molecular mechanisms of resistance, FEMS Microbiol. Rev. 33 (2009) 820-832.

642 [35] R.J. Turner, Y. Aharonowitz, J.H. Weiner, D.E. Taylor, Glutathione is a target in tellurite
643 toxicity and is protected by tellurite resistance determinants in Escherichia coli, Can. J.
644 Microbiol. 47 (2001) 33-40.

[36] U.B. Kavurt, M. Marioli, W.T. Kok, D. Stamatialis, Membranes for separation of biomacromolecules and bioparticles via flow field-flow fractionation, Journal of Chemical Technology & Biotechnology 90 (2015) 11-18.

[37] H. Dou, E.C. Jung, S. Lee, Factors affecting measurement of channel thickness in asymmetrical flow field-flow fractionation, Journal of Chromatography A 1393 (2015) 115-121.

[38] B. Meisterjahn, S. Wagner, F. von der Kammer, D. Hennecke, T. Hofmann, Silver and gold nanoparticle separation using asymmetrical flow-field flow fractionation: influence of run conditions and of particle and membrane charges, Journal of Chromatography A 1440 (2016) 150-159.

[39] Y. González-Espinosa, B. Sabagh, E. Moldenhauer, P. Clarke, F.M. Goycoolea, Characterisation of chitosan molecular weight distribution by multi-detection asymmetric flow-field flow fractionation (AF4) and SEC, Int. J. Biol. Macromol. 136 (2019) 911-919.

[40] D.A. Ladner, M. Steele, A. Weir, K. Hristovski, P. Westerhoff, Functionalized nanoparticle interactions with polymeric membranes, J. Hazard. Mater. 211-212 (2012) 288-295.

[41] V.R. Patel, Y.K. Agrawal, Nanosuspension: An approach to enhance solubility of drugs, J. Adv. Pharm. Technol. Res. 2 (2011) 81-87.

[42] S. Bhattacharjee, DLS and zeta potential–What they are and what they are not? J. Controlled Release 235 (2016) 337-351.

[43] H. Kouchakzadeh, S.A. Shojaosadati, A. Maghsoudi, E.V. Farahani, Optimization of PEGylation conditions for BSA nanoparticles using response surface methodology, Aaps Pharmscitech 11 (2010) 1206-1211.

[44] J.C. Giddings, F.J. Yang, M.N. Myers, Theoretical and experimental characterization of flow field-flow fractionation, Anal. Chem. 48 (1976) 1126-1132.

[45] M. Baalousha, F.V.D. Kammer, M. Motelica-Heino, H.S. Hilal, P. Le Coustumer, Size fractionation and characterization of natural colloids by flow-field flow fractionation coupled to multi-angle laser light scattering, Journal of Chromatography A 1104 (2006) 272-281.

[46] E. Alasonati, M. Benincasa, V.I. Slaveykova, Asymmetrical flow field-flow fractionation coupled to multiangle laser light scattering detector: Optimization of crossflow rate, carrier characteristics, and injected mass in alginate separation, Journal of separation science 30 (2007) 2332-2340.

[47] M. Leeman, K. Wahlund, B. Wittgren, Programmed cross flow asymmetrical flow field-flow fractionation for the size separation of pullulans and hydroxypropyl cellulose, Journal of Chromatography A 1134 (2006) 236-245.

[48] M. Andersson, B. Wittgren, K. Wahlund, Accuracy in multiangle light scattering measurements for molar mass and radius estimations. Model calculations and experiments, Anal. Chem. 75 (2003) 4279-4291.

[49] C. Ma, J. Yan, Y. Huang, C. Wang, G. Yang, The optical duality of tellurium nanoparticles for broadband solar energy harvesting and efficient photothermal conversion, Science advances 4 (2018) eaas9894.

[50] K.C. Nwoko, A. Raab, L. Cheyne, D. Dawson, E. Krupp, J. Feldmann, Matrix-dependent size modifications of iron oxide nanoparticles (Ferumoxytol) spiked into rat blood cells and plasma: Characterisation with TEM, AF4-UV-MALS-ICP-MS/MS and spICP-MS, Journal of Chromatography B 1124 (2019) 356-365.

[51] J. Jiménez-Lamana, I. Abad-Álvaro, K. Bierla, F. Laborda, J. Szpunar, R. Lobinski, Detection and characterization of biogenic selenium nanoparticles in selenium-rich yeast by single particle ICPMS, J. Anal. At. Spectrom. 33 (2018) 452-460.

[52] G. Cornelis, M. Hassellöv, A signal deconvolution method to discriminate smaller nanoparticles in single particle ICP-MS, J. Anal. At. Spectrom. 29 (2014) 134-144.

[53] B. Gómez-Gómez, J. Sanz-Landaluce, M.T. Pérez-Corona, Y. Madrid, Fate and effect of in-house synthesized tellurium-based nanoparticles on bacterial biofilm biomass and architecture. Challenges for nanoparticles characterization in living systems, Science of The Total Environment 719 (2020) 137501.

[54] S. Tsuneda, H. Aikawa, H. Hayashi, A. Yuasa, A. Hirata, Extracellular polymeric substances responsible for bacterial adhesion onto solid surface, FEMS Microbiol. Lett. 223 (2003) 287-292.

[55] G.H. Woehrle, J.E. Hutchison, S. Özkar, R.G. FINKE, Analysis of nanoparticle transmission electron microscopy data using a public-domain image-processing program, image, Turkish Journal of Chemistry 30 (2006) 1-13.

[56] R. Pecora, Dynamic light scattering measurement of nanometer particles in liquids, Journal of nanoparticle research 2 (2000) 123-131.

[57] R. Peters, Y. Georgalis, W. Saenger, Accessing lysozyme nucleation with a novel dynamic light scattering detector, Acta Crystallographica Section D: Biological Crystallography 54 (1998) 873-877.

[58] X.Z. Wang, L. Liu, R.F. Li, R.J. Tweedie, K. Primrose, J. Corbett, F.K. McNeil-Watson, Online characterisation of nanoparticle suspensions using dynamic light scattering, ultrasound spectroscopy and process tomography, Chemical Engineering Research and Design 87 (2009) 874-884.

[59] M.M. Tosi, A.P. Ramos, B.S. Esposto, S.M. Jafari, in Anonymous Dynamic light scattering (DLS) of nanoencapsulated food ingredients. Characterization of Nanoencapsulated Food Ingredients. Elsevier, 2020, p. 191-211.

718 [60] A. Moquin, F.M. Winnik, in Anonymous The use of field-flow fractionation for the
719 analysis of drug and gene delivery systems. Field-Flow Fractionation in Biopolymer Analysis.
720 Springer, 2012, p. 187-206.

721 [61] S.R. Ravella, T.S. Quiñones, A. Retter, M. Heiermann, T. Amon, P.J. Hobbs, Extracellular
722 polysaccharide (EPS) production by a novel strain of yeast-like fungus Aureobasidium
723 pullulans, Carbohydrate Polymers 82 (2010) 728-732.

724 [62] S. Valueva, M. Vylegzhanina, V. Lavrent'ev, L. Borovikova, T. Sukhanova, Biogenic
725 nanosized systems based on selenium nanoparticles: Self-organization, structure, and
726 morphology, Russian Journal of Physical Chemistry A 87 (2013) 484-489.

727 [63] J. Liu, C. Liang, X. Zhu, Y. Lin, H. Zhang, S. Wu, Understanding the solvent molecules
728 induced spontaneous growth of uncapped tellurium nanoparticles, Scientific reports 6
729 (2016) 32631.

730 [64] D. Ruhland, K. Nwoko, M. Perez, J. Feldmann, E.M. Krupp, AF4-UV-MALS-ICP-MS/MS,
731 spICP-MS, and STEM-EDX for the Characterization of Metal-Containing Nanoparticles in Gas
732 Condensates from Petroleum Hydrocarbon Samples, Anal. Chem. 91 (2018) 1164-1170.

733 [65] B. Hetzer, A. Burcza, V. Gräf, E. Walz, R. Greiner, Online-coupling of AF4 and single
734 particle-ICP-MS as an analytical approach for the selective detection of nanosilver release
735 from model food packaging films into food simulants, Food Control 80 (2017) 113-124.

736 [66] B. Bocca, B. Battistini, F. Petrucci, Silver and gold nanoparticles characterization by SP-
737 ICP-MS and AF4-FFF-MALS-UV-ICP-MS in human samples used for biomonitoring, Talanta
738 220 (2020) 121404.

Figure

Click here to access/download;Figure;Figure 1.docx

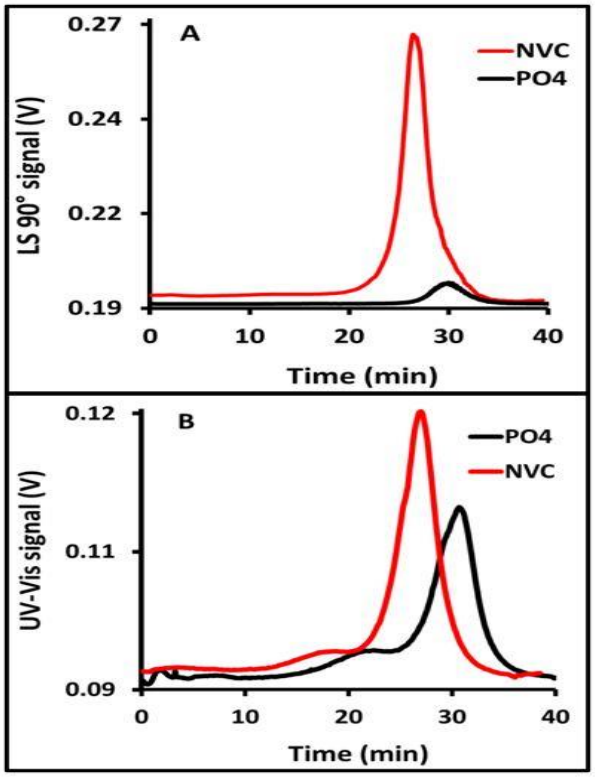

Figure

Click here to access/download;Figure;Figure 2.docx

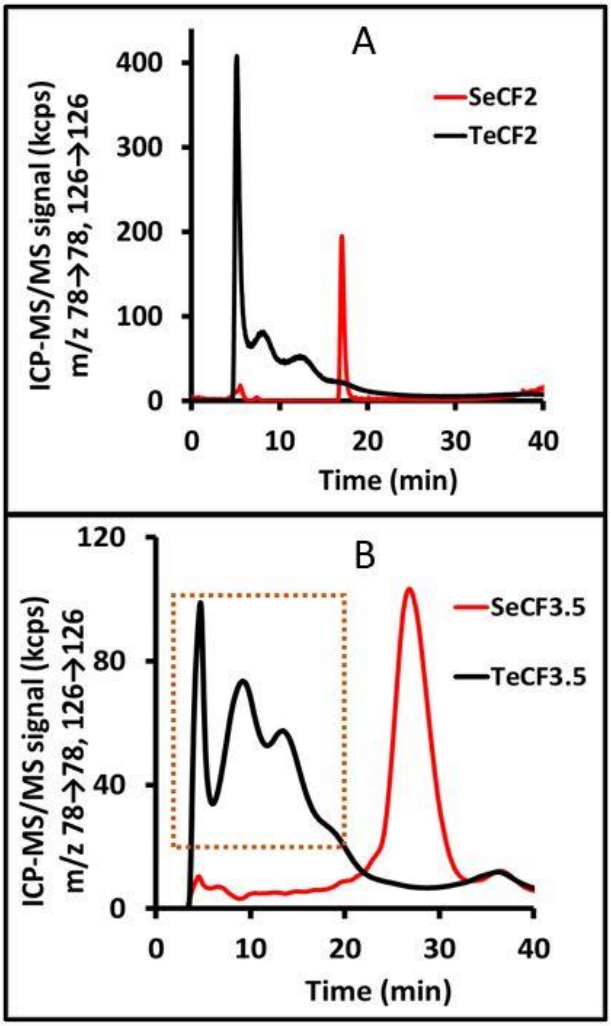

Figure

Click here to access/download;Figure;Figure 3.docx

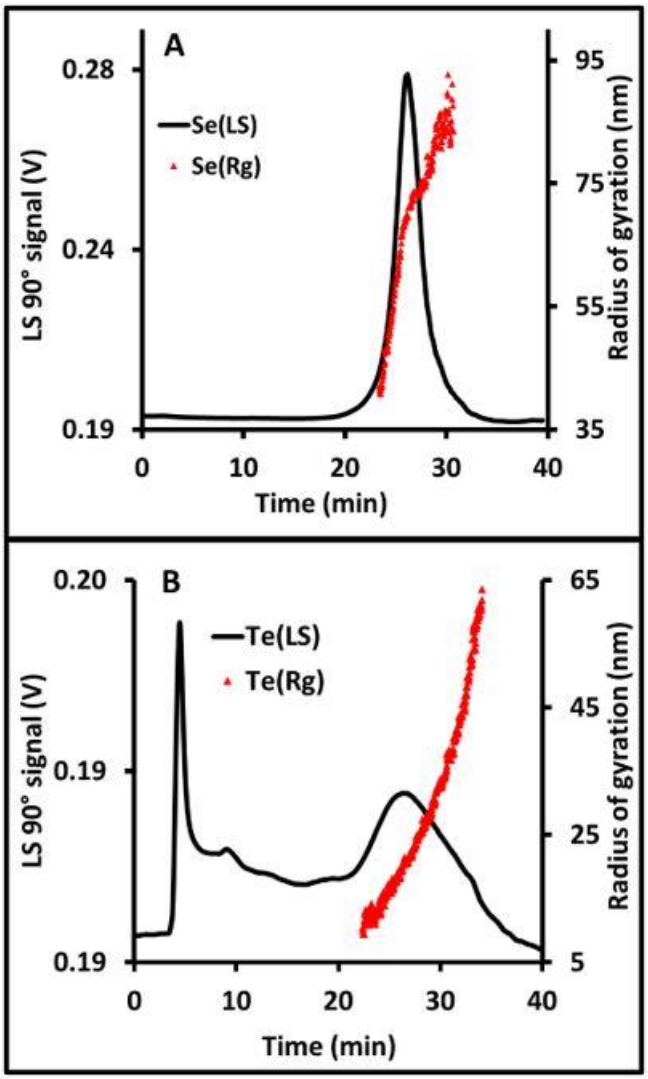

Figure

Click here to access/download;Figure;Figure 4.docx

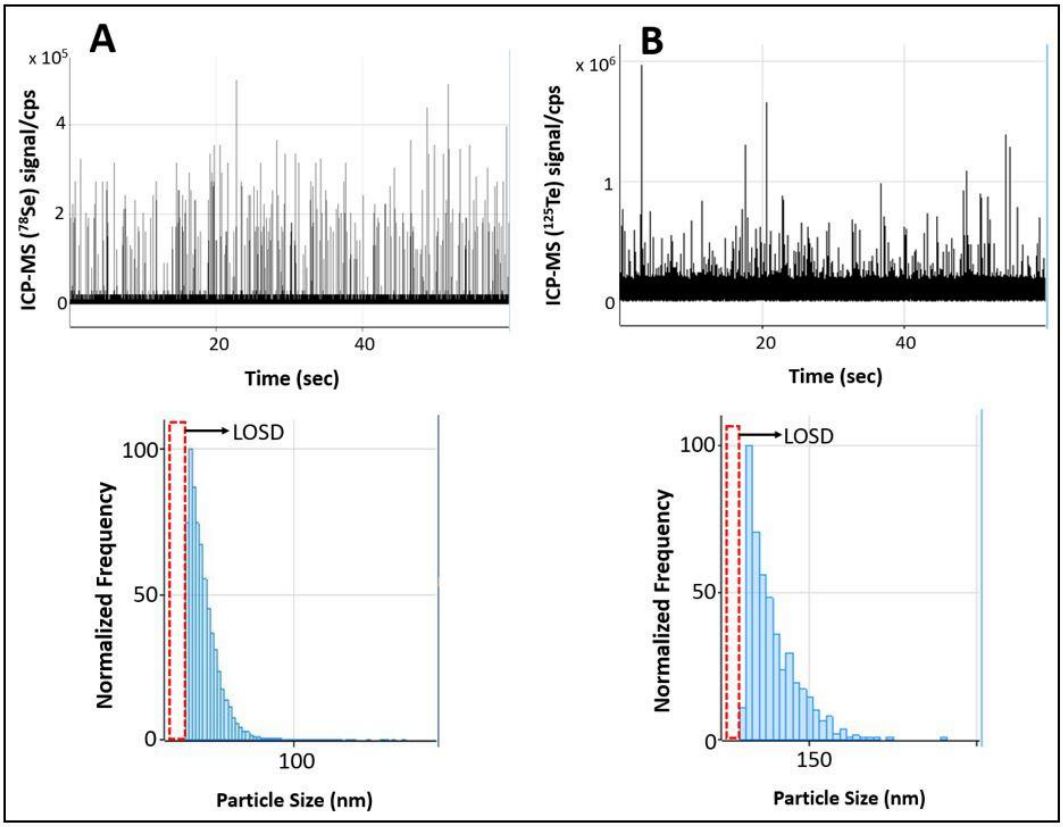

Figure

Click here to access/download;Figure;Figure 5.docx

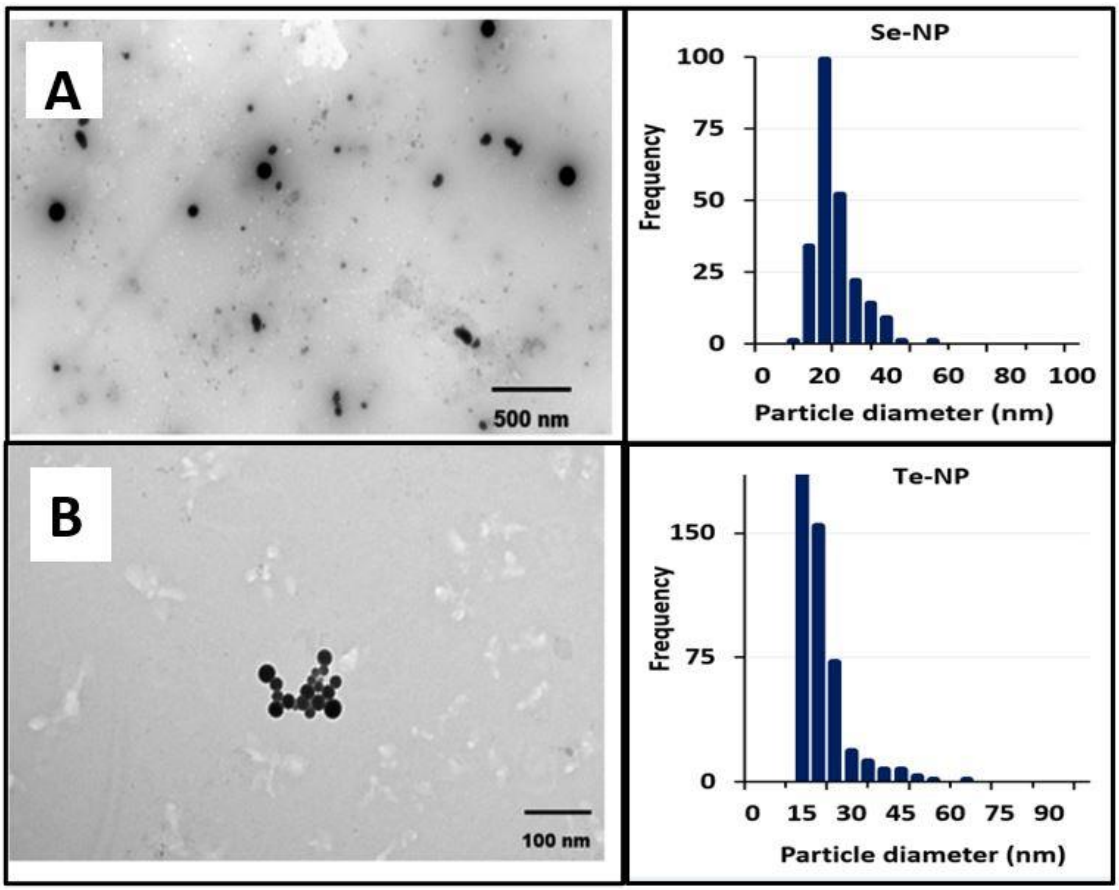

Figure

Click here to access/download;Figure;Figure 6.docx

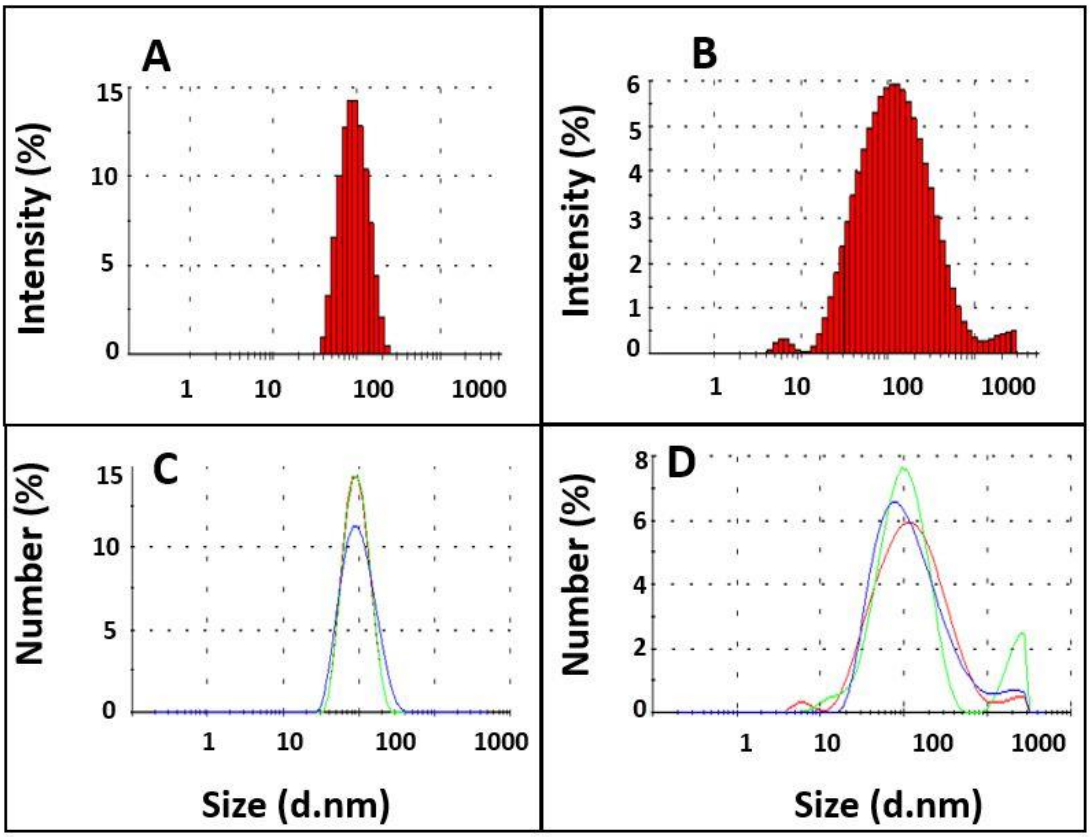

Table 1. ZP values of Se-NP and Te-NP dispersed in AF4 running solutions.

Dispersant	**Se-NP (mV)**	**Te-NP (mV)**
Novachem	-38	-27
Phosphate buffer	-18	-11

Table 2. Summary of particle sizes measured with the different techniques. Errors are given as standard deviation of triplicates; diameters and mathematical radius are shown (in parentheses).

NP	**AF4-MALS (Mean R_g)**	**spICP-MS**	**TEM**	**DLS (D_H)**
Se-NP	80.0± 0.4 nm	49.7±2.7 nm (25 nm)	35.5±2.5 nm (17.8 nm)	167±0.9 nm (83.5 nm)
Te-NP	29.5±0.6 nm	135±4.3 nm (67.5 nm)	39.0±1.9 nm (19.5 nm)	174±3.1 nm (87 nm)

CRediT Author Statement

Kenneth C Nwoko: Writing-original draft, review and editing, sample preparation, instrumental analysis (AF4-UV-MALS-ICP-MS/MS), DLS, TEM.

Xinjin Liang: Growth and culture experiments, review, editing.

Magali AMJ Perez: Sample preparation and instrumental analysis (spICP-MS, TEM).

Eva Krupp: Supervision.

Geoffrey Michael Gadd: Conceptualization, supervision, funding acquisition, review, editing.

Jörg Feldmann: Conceptualization, supervision, funding acquisition, review, editing.

*Conflict of Interest Statement

Declaration of interests

☒ The authors declare that they have no known competing financial interests or personal relationships that could have appeared to influence the work reported in this paper.

☐The authors declare the following financial interests/personal relationships which may be considered as potential competing interests: